

## Copper(I)/O<sub>2</sub> Chemistry with Imidazole Containing Tripodal Tetradentate Ligands Leading to $\mu$ -1,2-Peroxo–Dicopper(II) Species

Yunho Lee,<sup>†</sup> Ga Young Park,<sup>†</sup> Heather R. Lucas,<sup>†</sup> Peter L. Vajda,<sup>†</sup> Kaliappan Kamaraj,<sup>†</sup> Michael A. Vance,<sup>‡</sup> Ashley E. Milligan,<sup>‡</sup> Julia S. Woertink,<sup>‡</sup> Maxime A. Siegler,<sup>†</sup> Amy A. Narducci Sarjeant,<sup>†,||</sup> Lev N. Zakharov,<sup>§,⊥</sup> Arnold L. Rheingold,<sup>§,⊗</sup> Edward I. Solomon,<sup>\*,‡</sup> and Kenneth D. Karlin<sup>\*,†</sup>

<sup>†</sup>Department of Chemistry, The Johns Hopkins University, Baltimore, Maryland 21218, <sup>‡</sup>Department of Chemistry, Stanford University, Stanford, California 94305, and <sup>§</sup>Department of Chemistry, University of Delaware, Newark, Delaware 19716. <sup>||</sup>Current address: Department of Chemistry, Northwestern University, Evanston IL. <sup>⊥</sup>Current address: Department of Chemistry, University of Oregon, Eugene OR. <sup>⊗</sup>Current address: Department of Chemistry and Biology, UCSD, La Jolla, CA.

Received September 8, 2009

Cuprous and cupric complexes with the new imidazolyl containing tripodal tetradentate ligands  $\{L^{MIm}, (1H\text{-imidazol-4-yl})\text{-}N,N\text{-bis}(\text{pyridin-2-yl})\text{methylmethanamine, and } L^{EIm}, 2\text{-}(1H\text{-imidazol-4-yl})\text{-}N,N\text{-bis}(\text{pyridin-2-yl})\text{methyl ethanamine}\}$ , have been investigated to probe differences in their chemistry, especially in copper(I)–dioxygen chemistry, compared to that already known for the pyridyl analogue TMPA, tris(2-pyridyl)methylamine. Infrared (IR) stretching frequencies obtained from carbon monoxide adducts of  $[(L^{MIm})Cu^I]^+$  (**1a**) and  $[(L^{EIm})Cu^I]^+$  (**2a**) show that the imidazolyl donor is stronger than its pyridyl analogue. Electrochemical data suggest differences in the binding constant of Cu<sup>II</sup> to L<sup>EIm</sup> compared to TMPA and L<sup>MIm</sup>, reflecting geometric changes. Oxygenation of  $[(L^{MIm})Cu^I]^+$  (**1a**) in 2-methyltetrahydrofuran (MeTHF) solvent at  $-128^\circ\text{C}$  leads to an intensely purple colored species with a UV–vis spectrum characteristic of an end-on bound peroxodicopper(II) complex  $[\{(L^{MIm})Cu^{II}\}_2(\mu\text{-}1,2\text{-O}_2^{2-})]^{2+}$  (**1b<sup>P</sup>**)  $\{\lambda_{\text{max}}=528\text{ nm}\}$ , very similar to the previously well characterized complex  $[\{(TMPA)Cu^{II}\}_2(\mu\text{-}1,2\text{-O}_2^{2-})]^{2+}$   $\{\lambda_{\text{max}}=520\text{ nm} (\epsilon=12\,000\text{ M}^{-1}\text{ cm}^{-1}), \text{ in MeTHF; resonance Raman (rR) spectroscopy: } \nu(\text{O}=\text{O})=832 (\Delta(^{18}\text{O}_2)=-44)\text{ cm}^{-1}\}$ . In the low-temperature oxygenation of **2a**, benchtop ( $-128^\circ\text{C}$ ) and stopped-flow ( $-90^\circ\text{C}$ ) experiments reveal the formation of an initial superoxo-Cu(II) species  $[(L^{EIm})Cu^{II}(\text{O}_2^{\bullet-})]^+$  (**2b<sup>S</sup>**),  $\lambda_{\text{max}}=431\text{ nm}$  in THF). This converts to the low-temperature stable peroxo complex  $[\{(L^{EIm})Cu^{II}\}_2(\mu\text{-}1,2\text{-O}_2^{2-})]^{2+}$  (**2b<sup>P</sup>**)  $\{\text{rR spectroscopy: } \nu(\text{O}=\text{O})=822 (\Delta(^{18}\text{O}_2)=-46)\text{ cm}^{-1}\}$ . Complex **2b<sup>P</sup>** possess distinctly reduced Cu–O and O–O stretching frequencies and a red-shifted UV–vis feature  $\{\text{to } \lambda_{\text{max}}=535\text{ nm} (\epsilon=11\,000\text{ M}^{-1}\text{ cm}^{-1})\}$  compared to the TMPA analogue due to a distortion from trigonal bipyramidal (TBP) to a square pyramidal ligand field. This distortion is supported by the structural characterization of related ligand–copper(II) complexes: A stable tetramer cluster complex  $[(\mu_2\text{-}L^{EIm})_4\text{-}(\text{Cu}^{II})_4]^{4+}$ , obtained from thermal decomposition of **2b<sup>P</sup>** (with formation of H<sub>2</sub>O<sub>2</sub>), also exhibits a distorted square pyramidal Cu(II) ion geometry as does the copper(II) complex  $[(L^{EIm})Cu^{II}(\text{CH}_3\text{CN})]^{2+}$  (**2c**), characterized by X-ray crystallography and solution electron paramagnetic resonance (EPR) spectroscopy.

### Introduction

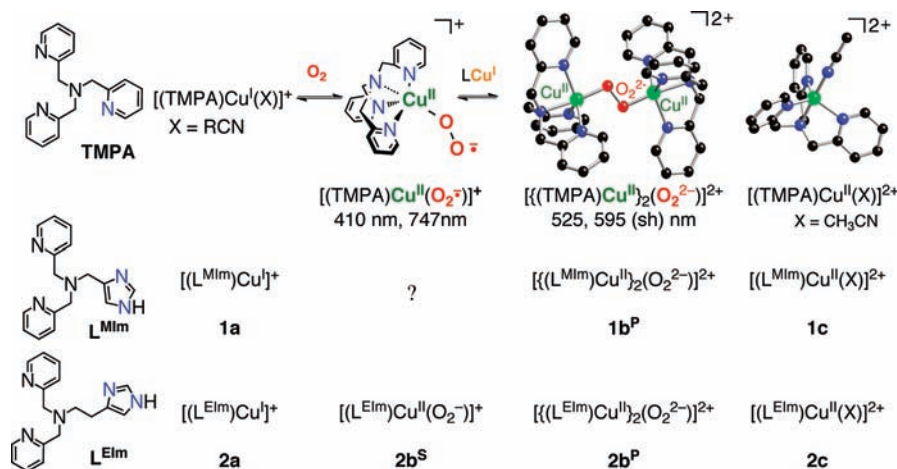
In this Article, we present detailed studies of the copper(I)–dioxygen reactivity of new complexes containing tripodal tetradentate ligands L<sup>MIm</sup> and L<sup>EIm</sup> (Scheme 1), possessing one imidazolyl group. We compare and contrast the reactivity and physical properties of the resulting dioxygen adducts with

those known with the previously well-studied close analogue ligand TMPA (tris(2-pyridylmethyl)amine).<sup>1–7</sup> The study of copper–dioxygen adduct formation, structures, physical properties, and subsequent reactivity is an area of active research, since the acquisition of fundamental insights into this subject is of considerable chemical and bioinorganic interest.<sup>1–3,8</sup>

\*To whom correspondence should be addressed. E-mail: karlin@jhu.edu.  
(1) Hatcher, L. Q.; Karlin, K. D. *J. Biol. Inorg. Chem.* **2004**, *9*, 669–683.  
(2) Mirica, L. M.; Ottenwaelder, X.; Stack, T. D. P. *Chem. Rev.* **2004**, *104*, 1013–1045.  
(3) Lewis, E. A.; Tolman, W. B. *Chem. Rev.* **2004**, *104*, 1047–1076.  
(4) Jacobson, R. R.; Tyeklar, Z.; Karlin, K. D.; Liu, S.; Zubieta, J. *J. Am. Chem. Soc.* **1988**, *110*, 3690–3692.

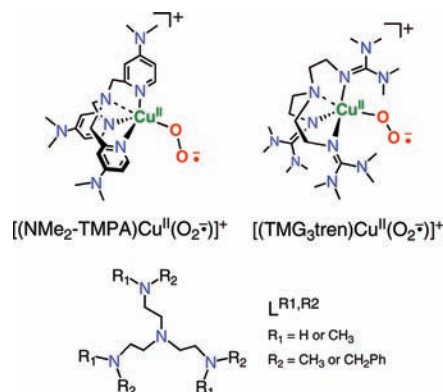
(5) Tyeklar, Z.; Jacobson, R. R.; Wei, N.; Murthy, N. N.; Zubieta, J.; Karlin, K. D. *J. Am. Chem. Soc.* **1993**, *115*, 2677–2689.  
(6) Baldwin, M. J.; Ross, P. K.; Pate, J. E.; Tyeklar, Z.; Karlin, K. D.; Solomon, E. I. *J. Am. Chem. Soc.* **1991**, *113*, 8671–8679.  
(7) Karlin, K. D.; Kaderli, S.; Zuberbühler, A. D. *Acc. Chem. Res.* **1997**, *30*, 139–147.  
(8) Itoh, S. *Curr. Opin. Chem. Biol.* **2006**, *10*, 115–122.

Scheme 1



Detailed kinetic-mechanistic and structural studies show that the  $\mu$ -1,2-end-on peroxo dicopper(II) complex  $[\{(TMPA)Cu^{II}\}_2(O_2^{2-})]^{2+}$  (Scheme 1) forms via a reversible reaction between an initially formed  $Cu^{II}$ -superoxo intermediate ( $\lambda_{max} = 410$  nm, also formed reversibly) with a second TMPA-cuprous complex (Scheme 1).<sup>7,9,10</sup> The intensely purple colored  $[\{(TMPA)Cu^{II}\}_2(O_2^{2-})]^{2+}$  shows absorption features [ $\lambda_{max}$  nm ( $\epsilon$   $cm^{-1}$   $M^{-1}$ )] at 440 (4 000), 525 (11 500), and 590 (7 600) in EtCN at  $-80$  °C, which have been assigned as ligand(peroxide)-to-metal charge-transfer (LMCT) bands.<sup>6</sup> The formation of an end-on bound dioxygen adduct (as a peroxide species) was confirmed structurally (Scheme 1), with each copper(II) ion in a trigonal bipyramidal coordination environment with  $Cu \cdots Cu = 4.359$  Å and  $O-O = 1.432$  Å, the latter value typical for peroxides.<sup>4</sup> The peroxo-dicopper(II) formulation was further confirmed by resonance Raman (rR) spectroscopy,  $\nu(O-O) = 832$  ( $\Delta(^{18}O_2) = -44$ )  $cm^{-1}$ .<sup>6</sup> In the context of this discussion of the superoxo-copper(II) or peroxodicopper(II) complexes with TMPA as a ligand, there have been notable relevant recent advances: (i) The copper(I) carbonyl complex of a TMPA analogue with  $Me_2N$  substituents at the 4-pyridyl position reacts to form a stable  $-80$  °C solution complex  $[(Me_2N-TMPA)Cu^{II}(O_2^{\cdot-})]^+$  species, spectroscopically proven to possess an end-on superoxide binding (diagram).<sup>11</sup> (ii) Strikingly, Schindler and co-workers<sup>12</sup> crystallized and structurally characterized a related complex  $[(TMG_3tren)Cu^{II}(O_2^{\cdot-})]^+$  (diagram). (iii) With all alkylamino containing  $N_4$  tripodal tetradentate ligands ( $L^{R_1,R_2}$  in diagram), Suzuki and co-workers<sup>13</sup> spectroscopically detailed related superoxo- $Cu^{II}$  complexes and crystallographically described a

$\mu$ -1,2-peroxodicopper(II) complex analogue of  $[\{(TMPA)Cu^{II}\}_2(O_2^{2-})]^{2+}$ .



We and others have extensively employed pyridyl donors as part of tridentate or tetradentate chelating ligands for copper(I), for their synthetic ease and behavior toward promoting copper(I)/dioxygen reactivity of considerable interest.<sup>1-3,8,14</sup> Here, our choice of ligands  $L^{MIm}$  and  $L^{EIm}$  ( $\{L^{MIm}, (1H\text{-imidazol-4-yl})\text{-}N,N\text{-bis}((\text{pyridin-2-yl})\text{methyl})\text{-methanamine}; L^{EIm}, 2\text{-}(1H\text{-imidazol-4-yl})\text{-}N,N\text{-bis}((\text{pyridin-2-yl})\text{methyl})\text{ethanamine (Scheme 1)}\}$  derives from interest in studying an imidazolyl moiety as a copper ion ligand, which more closely resembles protein histidine ligand groups (as linked in the 4(5)-position). In fact, imidazolyl containing ligands have been studied in copper coordination chemistry.<sup>15-24</sup> A few examples exist where  $LCu^I/O_2$  studies

(9) Zhang, C. X.; Kaderli, S.; Costas, M.; Kim, E.-i.; Neuhold, Y.-M.; Karlin, K. D.; Zuberbühler, A. D. *Inorg. Chem.* **2003**, *42*, 1807-1824.

(10) Fry, H. C.; Scaltrito, D. V.; Karlin, K. D.; Meyer, G. J. *J. Am. Chem. Soc.* **2003**, *125*, 11866-11871.

(11) Maiti, D.; Fry, H. C.; Woertink, J. S.; Vance, M. A.; Solomon, E. I.; Karlin, K. D. *J. Am. Chem. Soc.* **2007**, *129*, 264-265.

(12) Würtele, C.; Gaoutchenova, E.; Harms, K.; Holthausen, M. C.; Sundermeyer, J.; Schindler, S. *Angew. Chem., Int. Ed.* **2006**, *45*, 3867-3869.

(13) Komiyama, K.; Furutachi, H.; Nagatomo, S.; Hashimoto, A.; Hayashi, H.; Fujinami, S.; Suzuki, M.; Kitagawa, T. *Bull. Chem. Soc. Jpn.* **2004**, *77*, 59-72.

(14) Hatcher, L. Q.; Karlin, K. D. *Adv. Inorg. Chem.* **2006**, *58*, 131-184.

(15) Battaini, G.; Monzani, E.; Perotti, A.; Para, C.; Casella, L.; Santagostini, L.; Gullotti, M.; Dillinger, R.; Nather, C.; Tuzcek, F. *J. Am. Chem. Soc.* **2003**, *125*, 4185-4198.

(16) Itoh, K.; Hayashi, H.; Furutachi, H.; Matsumoto, T.; Nagatomo, S.; Tosha, T.; Terada, S.; Fujinami, S.; Suzuki, M.; Kitagawa, T. *J. Am. Chem. Soc.* **2005**, *127*, 5212-5223.

(17) Cheruzel, L. E.; Cecil, M. R.; Edison, S. E.; Mashuta, M. S.; Baldwin, M. J.; Buchanan, R. M. *Inorg. Chem.* **2006**, *45*, 3191-3202.

(18) Cheruzel, L. E.; Mashuta, M. S.; Buchanan, R. M. *Chem. Commun.* **2005**, 2223-2225.

(19) Beretta, M.; Bouwman, E.; Casella, L.; Douzich, B.; Driessen, W. L.; Gutierrez-Soto, L.; Monzani, E.; Reedijk, J. *Inorg. Chim. Acta* **2000**, *310*, 41-50.

(20) Santagostini, L.; Gullotti, M.; Pagliarini, R.; Bianchi, E.; Casella, L.; Monzani, E. *Tetrahedron: Asymmetry* **1999**, *10*, 281-295.

were carried out,<sup>25–29</sup> but they have generally not afforded new insights with respect to characterization of copper–dioxygen adducts.

In the present study employing  $L^{MIm}$  and  $L^{EIm}$ , we have synthesized new copper(I) complexes (**1a** and **2a** in Scheme 1), spectroscopically characterized peroxy–dicopper(II) complexes (**1b<sup>P</sup>** and **2b<sup>P</sup>** in Scheme 1) and have detected and partially characterized a superoxy–copper(II) complex with  $L^{EIm}$  (**2b<sup>S</sup>** in Scheme 1). Stable copper(II) complexes (**1c** and **2c** in Scheme 1) have also been synthesized and characterized to probe the geometric effect of the new ligands on the copper(II) centers. Insights obtained from these structures aid the interpretation of spectroscopic variations observed for the peroxy–dicopper(II) species, as detailed below.

## Experimental Section

**General Considerations and Instrumentation.** All reagents and solvents used for this work were commercial products and are of reagent quality unless otherwise stated. Acetonitrile ( $CH_3CN$ ), dichloromethane ( $CH_2Cl_2$ ), diethylether ( $Et_2O$ ), methanol ( $CH_3OH$ ), and tetrahydrofuran (THF) were purified and dried by passing through a double alumina column solvent purification system by Innovative Technologies, Inc. Anhydrous 2-methyltetrahydrofuran (MeTHF, packaged under nitrogen in Sure/Seal bottles, 99+%) was purchased from Sigma-Aldrich, Inc. Deoxygenation of these solvents was achieved by bubbling Ar for 30 min and/or carrying out three freeze/pump/thaw cycles. Air-sensitive compounds were handled under an Ar atmosphere using standard Schlenk techniques or within a MBraun Labmaster 130 inert-atmosphere ( $N_2$  atmosphere; <1 ppm  $O_2$ , <1 ppm  $H_2O$ ) glovebox. Molecular oxygen (Airgas Inc., Radnor, PA) was dried by passing it through a laboratory gas drying unit (W. A. Hammond Drierite Co., Xenia, Ohio) and introduced to reaction solutions by bubbling through an 18-gauge, 24 inch-long stainless steel syringe needle.  $[Cu^I(CH_3CN)_4]ClO_4$  and  $[Cu^I(CH_3CN)_4]B(C_6F_5)_4$  were prepared by literature procedures.<sup>30,31</sup>  $KB(C_6F_5)_4$  or  $LiB(C_6F_5)_4$  were purchased from Boulder Scientific Company.

**Warning:** While we have experienced no problems in working with perchlorate compounds, they are potentially explosive, and care must be taken not to work with large quantities.

**<sup>1</sup>H Nuclear Magnetic Resonance (NMR) and <sup>13</sup>C NMR.** <sup>1</sup>H NMR and <sup>13</sup>C NMR spectra were measured on a Varian 400 MHz or Bruker 400 MHz spectrometer, and chemical shifts are

reported in ppm ( $\delta$ ) downfield from an internal TMS ( $Me_4Si$ ) reference and the residual solvent proton peak.

**Infrared Spectra.** Infrared spectra were recorded on a Mattson Instruments 4030 Galaxy series Fourier transform-infrared (FT-IR) spectrometer. Measuring the solution IR spectra of carbonyl adducts (as a solution in THF) were recorded using standard solution IR cells. Air sensitive cuprous THF solutions were prepared in a glovebox ( $N_2$  filled, MBraun) and then removed using 20 mL vials sealed with a 14/20 rubber septum. Carbon monoxide gas (Airgas Inc., Radnor, PA) was introduced to the corresponding solution via bubbling for 20–30 s through an 18-gauge, 24-in.-long stainless steel syringe needle. The resulting solution was transferred to a solution IR cell by the gastight syringe under the CO atmosphere.

**Elemental Analyses.** Elemental analyses were performed by Desert Analytics, Tucson, AZ, for air-sensitive samples or by Quantitative Technologies Inc. (QTI), Whitehouse, NJ, for others.

**Mass Spectrometry.** Mass spectrometry was conducted at the mass spectrometry facility either at the Johns Hopkins University or at the Ohio State University. Chemical Ionization (CI) and fast atomic bombardment (FAB) mass spectra were acquired at the Johns Hopkins University facility using a VG70S double focusing magnetic sector mass spectrometer (VG Analytical, Manchester, U.K., now Micromass/Waters) equipped with a Xe gas FAB gun (8 kV at 1.2 mA) and an off-axis electron multiplier and an MSS data system (MasCom, Bremen, Germany). The resolution of the instrument was set at 10 000 (100 ppm peak width). Samples were mixed with *m*-nitrobenzyl–alcohol matrix deposited on the target of a direct insertion probe for introduction into the source. Nominal mass scan spectra were acquired with a mass scan range of 10–950 amu using a magnet scan rate of 25 second/decade. For accurate mass measurements, a narrower mass scan range was employed, with the matrix containing 10% PEG mass calibrant. ESI mass spectra (Johns Hopkins University facility) were acquired using a Finnigan LCQDeca ion-trap mass spectrometer equipped with an electrospray ionization source (Thermo Finnigan, San Jose, CA). Samples were dissolved in  $CH_3OH$  or  $CH_3CN$  and introduced into the instrument at a rate of 10  $\mu$ L/min using a syringe pump via a silica capillary line. The heated capillary temperature was 250 °C, and the spray voltage was 5 kV. High-resolution electrospray ionization (ESI) mass spectrometry analyses were performed at the Ohio State University (MS) facility with a 3 T Finnigan FTMS-2000 Fourier transform mass spectrometer (FTMS). Samples were sprayed from a commercial Analytical electrospray ionization source and then focused into the FTMS cell using a home-built set of ion optics.

**Electrical Conductivity.** Electrical conductivity measurements<sup>32,33</sup> for the Cu(I) complexes  $[(TMPA)Cu^I(CH_3CN)]^+$ ,  $[(L^{MIm})Cu^I]^+$  (**1a**), and  $[(L^{EIm})Cu^I]^+$  (**2a**) were carried out in dimethylformamide (DMF) solvent using an Accumet AR20 pH/conductivity meter (Fisher Scientific) with the Accumet Immersion-type four-cell glass conductivity probe (cell constant  $\kappa = 1.0 \text{ cm}^{-1}$ ). Air sensitive cuprous DMF solutions (1 mM, 20 mL) were prepared in a glovebox ( $N_2$  filled, MBraun) and then removed using five drum vials sealed with a cap and electrical tape. The data were collected from measurements with continuous strong (over the top) Ar flow.

**Cyclic Voltammetry.** Cyclic voltammetry measurements were undertaken in  $CH_3CN$  and DMF using a BAS 100B electrochemical analyzer with a glassy carbon working electrode and a platinum wire auxiliary electrode. Potentials were recorded versus a Ag/AgNO<sub>3</sub> electrode. The voltammograms are plotted versus the  $Fe(Cp)_2^{+/0}$  potential which was measured as an external standard. Scans were run at 50–200 mV/s under an

(21) Nie, H. L.; Aubin, S. M. J.; Mashuta, M. S.; Porter, R. A.; Richardson, J. F.; Hendrickson, D. N.; Buchanan, R. M. *Inorg. Chem.* **1996**, *35*, 3325–3334.

(22) Chen, S.; Richardson, J. F.; Buchanan, R. M. *Inorg. Chem.* **1994**, *33*, 2376–2382.

(23) Sorrell, T. N.; Vankai, V. A.; Garrity, M. L. *Inorg. Chem.* **1991**, *30*, 207–210.

(24) Casella, L.; Gullotti, M.; Pallanza, G.; Ligoni, L. *J. Am. Chem. Soc.* **1988**, *110*, 4221–4227.

(25) Zhou, L.; Powell, D.; Nicholas, K. M. *Inorg. Chem.* **2006**, *45*, 3840–3842.

(26) Battaini, G.; Casella, L.; Gullotti, M.; Monzani, E.; Nardin, G.; Perotti, A.; Randaccio, L.; Santagostini, L.; Heinemann, F. W.; Schindler, S. *Eur. J. Inorg. Chem.* **2003**, 1197–1205.

(27) Sorrell, T. N.; Allen, W. E.; White, P. S. *Inorg. Chem.* **1995**, *34*, 952–960.

(28) Lynch, W. E.; Kurtz, D. M., Jr.; Wang, S.; Scott, R. A. *J. Am. Chem. Soc.* **1994**, *116*, 11030–11038.

(29) Wei, N.; Murthy, N. N.; Tyeklár, Z.; Karlin, K. D. *Inorg. Chem.* **1994**, *33*, 1177–1183.

(30) Liang, H.-C.; Kim, E.; Incarvito, C. D.; Rheingold, A. L.; Karlin, K. D. *Inorg. Chem.* **2002**, *41*, 2209–2212.

(31) Liang, H.-C.; Karlin, K. D.; Dyson, R.; Kaderli, S.; Jung, B.; Zuberbühler, A. D. *Inorg. Chem.* **2000**, *39*, 5884–5894.

(32) Geary, W. J. *Coord. Chem. Rev.* **1971**, *7*, 81–122.

(33) Sorrell, T. N.; Borovik, A. S. *J. Am. Chem. Soc.* **1987**, *109*, 4255–4260.

argon atmosphere using  $\sim 0.1$  M  $[\text{Bu}_4\text{N}][\text{PF}_6]$  as the supporting electrolyte.

**X-ray Crystallography.** X-ray cCrystallography was performed at the X-ray diffraction facility either at Johns Hopkins University or the University of Delaware (by the Prof. Arnold Rheingold group). A suitable green crystal of  $[(\text{L}^{\text{Mim}})\text{Cu}^{\text{II}}(\text{CH}_3\text{CN})]^{2+}$  (**1c**) was mounted with epoxy cement to the tip of a glass fiber. Intensity data were collected at 150(2) K with a Bruker SMART APEX CCD diffractometer with graphite-monochromated  $[\text{Mo K}\alpha]$  radiation ( $\lambda = 0.71073 \text{ \AA}$ ). An absorption correction was applied using the SADABS program (Sheldrick, G. M. SADABS (2.01), Bruker/Siemens Area Detector Absorption Correction Program, Bruker AXS, Madison, WI, 1998). The structure was solved using direct methods and refined using the Bruker *SHELXTL* (version 6.1) software package (Sheldrick, G.M. 2000). Suitable blue single crystals of  $[(\mu_2\text{-L}^{\text{EIm}})_4(\text{Cu}^{\text{II}})_4]^{4+}$  cluster and  $[(\text{L}^{\text{EIm}})\text{Cu}^{\text{II}}(\text{CH}_3\text{CN})(\text{OCIO}_3)]^+$  (**2c-OCIO<sub>3</sub>**) were mounted in Paratone-*N* oil on the end of a glass fiber and transferred to the  $\text{N}_2$  cold stream (110 K) of an Oxford Diffraction Xcalibur3 system equipped with Enhance optics  $[\text{Mo K}\alpha]$  radiation ( $\lambda = 0.71073 \text{ \AA}$ ) and a CCD detector. The frames were integrated and a face indexed absorption correction and an interframe scaling correction were also applied with the Oxford Diffraction *CrysAlisRED* software package (CrysAlis CCD, Oxford Diffraction Ltd., version 1.171.27p5 beta). The structures were solved using direct methods and refined using the Bruker *SHELXTL* (version 6.1) software package (Sheldrick, G.M. 2000).

**Low Temperature UV–Visible Spectra.** Low-temperature UV–vis spectra were obtained with either a Cary 50 Bio spectrophotometer equipped with a fiber optic coupler (Varian) and a fiber optic dip probe (Hellma, 661.302-QX-UV-2 mm-for-low-temperature) or a Hewlett-Packard model 8453 diode array spectrophotometer equipped with a custom-made quartz-wind-owed vacuum dewar filled with methanol ( $-80 \text{ }^\circ\text{C}$ ). A low temperature unit (Neslab ULT-95 low temperature circulator) is attached to the HP spectrophotometer via copper tubing. The methanol temperature within the dewar was monitored using a thermocouple probe (Omega model 651). For the low temperature measurements with a Cary 50 Bio spectrophotometer, a hexane/ $\text{N}_2(\text{l})$  bath ( $-94 \text{ }^\circ\text{C}$ ) or a pentane/ $\text{N}_2(\text{l})$  bath ( $-128 \text{ }^\circ\text{C}$ ) was used and the steady temperature was monitored with the type T thermocouple thermometer (model 650, Omega Engineering, CT). Air sensitive solutions were prepared in a glovebox ( $\text{N}_2$  filled, MBraun) and carried out in custom-made Schlenk tubes designed for the dip probe (Chemglass, JHU-0407-271MS) or Schlenk cuvettes. The cuvette assembly consisted of a two-window quartz cuvette (2 mm path) connected, via a 12 cm glass tube, to a 14/20 female ground glass joint. In order to calculate absorptivities at low temperature in MeTHF, a solvent contraction factor was calculated from the volume changes directly measured at different temperatures (10 mL at room temperature (RT) vs 8.53 mL at  $-128 \text{ }^\circ\text{C}$ ).

**Stopped-Flow Experiments.** Rapid kinetics were followed using a Hi-Tech Scientific SF-40 variable-temperature stopped-flow unit (2 mm or 1 cm path length cell, 2.5 mL syringe) with Teflon-lined stainless steel plumbing, combined with a TIDAS-MMS-VIS 500-3 diode array spectrometer (J&M, 256 diodes, 300–1100 nm, 0.8 ms minimum sampling time) using fiber bundle light guides connected to a CLH-20 halogen lamp (Zeiss, 20 W/12 V). The two glass coils, containing Cu(I) and dioxygen solutions, respectively, and the mixing chamber were immersed in an ethanol bath. This bath was placed in a Dewar, which was filled with liquid nitrogen for low-temperature measurements. The ethanol bath was cooled by liquid nitrogen evaporation, and its temperature was measured by using a Pt resistance thermocouple and maintained to 0.1 K by using a temperature-controlled thyristor power unit (both Hi-Tech). The concentrations of  $(\text{L}^{\text{EIm}})\text{Cu}(\text{I})$  solution used were 0.2 mM. The dioxygen concentration used was

4.0 mM. Data acquisition (up to 256 complete spectra, up to 4 different time bases) was performed by using the Kinspec program (J & M).

**Resonance Raman Experiments.** Resonance Raman (rR) spectra were obtained using a Princeton Instruments ST-135 back-illuminated CCD detector on a Spex 1877 CP triple monochromator with 1200, 1800, and 2400 grooves/mm holographic spectrograph gratings. Excitation was provided by a Coherent I90C-K  $\text{Kr}^+$  ion laser. The spectral resolution was  $< 2 \text{ cm}^{-1}$ . Sample concentrations were approximately 3–4 mM with respect to Cu (1.5–2 mM with respect to the dimer). The samples were cooled to 77 K in a quartz liquid nitrogen finger Dewar (Wilmad). Isotopic substitution was achieved by oxygenation with  $^{18}\text{O}_2$ .

**X-Band Electron Paramagnetic Resonance (EPR) Spectra.** X-Band EPR spectra were recorded on a Bruker EMX CW-EPR spectrometer controlled with a Bruker ER 041 XG microwave bridge operating at X-band ( $\sim 9 \text{ GHz}$ ). The low-temperature experiments were carried out via either a continuous-flow He(I) cryostat and ITC503 temperature controller made by Oxford Instruments, Inc. or  $\text{N}_2(\text{l})$  finger dewar.

**Synthesis of Ligands.**  $\text{L}^{\text{Mim}}$ . Bis(2-pyridylmethyl)amine (2.64 g, 13.2 mmol) and glacial acetic acid (2 mL) were added to 1*H*-imidazole-4-carbaldehyde (1.3 g, 13.3 mmol) methanol solution (100 mL). Sodium cyanoborohydride (1.3 g, 20.7 mmol) was slowly added to the yellow methanol solution with vigorous stirring. Reaction mixture was stirred at room temperature for 24 h under Ar. After acidification with concentrated hydrochloric acid, solvent was removed using a rotary evaporator and the resulting residue was dissolved in dichloromethane and washed with a saturated sodium carbonate solution. The organic layer was separated, dried over anhydrous  $\text{MgSO}_4$ , then filtered and concentrated under vacuum. The oil obtained (0.72 g, 2.45 mmol, 61%) was purified by column chromatography ( $\text{Al}_2\text{O}_3$ , ethylacetate/methanol (100:4),  $R_f = 0.3$ ).  $^1\text{H NMR}$  ( $\text{CDCl}_3$ ):  $\delta$  11.6 (s, 1H), 8.42 (d,  $J = 4 \text{ Hz}$ , 2H), 7.6 (m, 3H), 7.40 (d,  $J = 7.6 \text{ Hz}$ , 2H), 7.05 (m, 2H), 6.89 (s, 1H), 3.74 (s, 4H), 3.64 (s, 2H).  $^{13}\text{C NMR}$  ( $\text{CDCl}_3$ ):  $\delta$  159.0, 148.7, 136.6, 135.1, 123.4, 122.0, 59.2, 48.5. FAB mass spectrum:  $m/z$  280.2 ( $\text{M} + 1$ ) $^+$ .

**[4(5)-(2-Phthalimidoethyl)imidazole (a).** Histamine (1.6 g, 14.5 mmol) and phthalic anhydride (2.17 g, 14.7 mmol) were dissolved in ethanol (100 mL). After glacial acetic acid (20 mL) was introduced, the reaction mixture was refluxed for 4 h. The resulting mixture was cooled and solvent and acetic acid were removed using a rotary evaporator. Upon addition of ethanol (30 mL) to the resulting residue with vigorous stirring, a white precipitate formed. The white powder (3.3 g, 13.7 mmol, 95%) was collected by filtration, washed with cold ethanol, and dried under vacuum.  $^1\text{H NMR}$  ( $\text{CDCl}_3$ ):  $\delta$  13.4 (s, 1H), 8.4 (m, 4H), 8.19 (s, 1H), 7.46 (s, 1H), 4.42 (t,  $J = 7.4 \text{ Hz}$ , 2H), 3.47 (t,  $J = 7.4 \text{ Hz}$ , 2H).  $^{13}\text{C NMR}$  ( $\text{CDCl}_3$ ):  $\delta$  168.7 (CO), 135.9 (NCN), 135.3 (Im), 134.8 (Ar), 132.6 (Ar), 123.9 (Im), 117.4 (Ph), 26.6 ( $\text{CH}_2$ ), 22.1 ( $\text{CH}_2$ ).

**[4(5)-(2-Phthalimidoethyl)](triphenylmethyl)imidazole (b).** Compound **a** (3.47 g, 14.4 mmol) and triphenylmethylchloride (4.92 g, 17.6 mmol) were dissolved in DMF (15 mL), triethylamine (2.5 mL) was introduced, and the reaction mixture was stirred overnight at RT. After DMF was removed with a rotary evaporator, the resulting residue was dissolved in dichloromethane and washed with cold ethylacetate. The product oil (6.16 g, 12.7 mmol, 88%) was dried under vacuum, its purity was confirmed by thin layer chromatography (TLC) (silica gel, ethylacetate/hexane (1:1),  $R_f = 0.2$ ) and identified by NMR spectroscopy.  $^1\text{H NMR}$  ( $\text{CDCl}_3$ ):  $\delta$  7.77 (dd,  $J = 5.8, 3.2 \text{ Hz}$ , 2H), 7.70 (dd,  $J = 5.6, 2.8 \text{ Hz}$ , 2H), 7.25 (m, 10H), 7.05 (m, 6H), 6.52 (s, 1H), 3.88 (t,  $J = 7 \text{ Hz}$ , 2H), 2.86 (t,  $J = 7.2 \text{ Hz}$ , 2H).

**Triphenylmethylhistamine (c).** Compound **b** (8.22 g, 17.0 mmol) and hydrazine (2.3 mL, 73 mmol) were dissolved in ethanol (100 mL), and the reaction mixture was stirred overnight at RT under Ar. After the resulting residue was filtered, the

solvent was removed by rotary evaporation whereupon the organic mixture was dissolved in dichloromethane and washed with 1 N sodium hydroxide. After separation, the product oil (3.74 g, 10.6 mmol, 62%) was dried over anhydrous  $\text{MgSO}_4$ , filtered, and concentrated under vacuum.  $^1\text{H NMR}$  ( $\text{CDCl}_3$ ):  $\delta$  7.3 (m, 10H), 7.1 (m, 6H), 6.58 (s, 1H), 2.96 (t,  $J = 6.4$  Hz, 2H), 2.66 (t,  $J = 6.4$  Hz, 2H).

**Triphenylmethyl- $\text{L}^{\text{EIm}}$  (d).** Compound **c** (3.74 g, 10.6 mmol) and picolyl chloride hydrochloride (5.61 g, 34.2 mmol; previously washed with 1 N sodium hydroxide) were dissolved in dichloromethane (100 mL). After introduction of triethylamine (3 mL), the reaction mixture was refluxed under Ar for 3 days. After cooling to room temperature, more (~20 mL) of  $\text{CH}_2\text{Cl}_2$  was added and the solution was washed three times with brine. The organic layer was separated, dried over anhydrous  $\text{MgSO}_4$ , then filtered, and concentrated under vacuum. The product oil was obtained (5.03 g, 9.4 mmol, 88.8%) after purification by column chromatography ( $\text{Al}_2\text{O}_3$ , ethylacetate/methanol (100:2),  $R_f = 0.5$ ).  $^1\text{H NMR}$  ( $\text{CDCl}_3$ ):  $\delta$  8.36 (dm,  $J = 4$  Hz, 2H), 7.42 (t,  $J = 7.6$  Hz, 2H), 7.34 (d,  $J = 7.6$  Hz, 2H), 7.2 (m, 10H), 7.0 (m, 8H), 6.48 (s, 1H), 3.76 (s, 4H), 2.82 (t, 2H), 2.77 (t, 2H).  $^{13}\text{C NMR}$  ( $\text{CDCl}_3$ ):  $\delta$  160.2 (Py), 149.0 (Py), 142.7 (Im), 139.9 (Py), 138.3 (Im), 136.4 (Im), 129.9 (Ph), 128.1 (Ph), 128.0 (Ph), 122.8 (Ph), 121.9 (Py), 118.3 (Py), 75.2 (C), 60.6 (NCH<sub>2</sub>), 54.6 (CH<sub>2</sub>), 26.8 (CH<sub>2</sub>). FAB mass spectrum:  $m/z$  558.3 ( $\text{M} + \text{Na}$ )<sup>+</sup>.

**$\text{L}^{\text{EIm}}$ .** Compound **d** (2.14 g, 4.0 mmol) was dissolved in ethanol (100 mL). After glacial acetic acid (5% in ethanol) was introduced, the reaction mixture was refluxed for 1 h. After ethanol was removed using a rotary evaporator, the resulting residue was dissolved in dichloromethane and washed with a saturated sodium carbonate solution. The organic layer was separated, dried over anhydrous  $\text{MgSO}_4$ , then filtered, and concentrated under vacuum. The oil obtained (0.72 g, 2.45 mmol, 61%) was purified by column chromatography ( $\text{Al}_2\text{O}_3$ , ethylacetate/methanol (100:4),  $R_f = 0.3$ ).  $^1\text{H NMR}$  ( $\text{CDCl}_3$ ):  $\delta$  13 (s, 1H), 8.44 (dm,  $J = 4.8$  Hz, 2H), 7.56 (s, 1H), 7.45 (dt,  $J = 7.8, 1.7$  Hz, 2H), 7.0 (m, 4H), 6.66 (s, 1H), 3.76 (s, 4H), 2.77 (m, 4H).  $^{13}\text{C NMR}$  ( $\text{CDCl}_3$ ):  $\delta$  159.4, 149.0, 136.8, 134.8, 123.4, 122.4, 60.0, 54.1, 23.4. FAB mass spectrum:  $m/z$  294.3 ( $\text{M} + 1$ )<sup>+</sup>, 316.4 ( $\text{M} + \text{Na}$ )<sup>+</sup>.

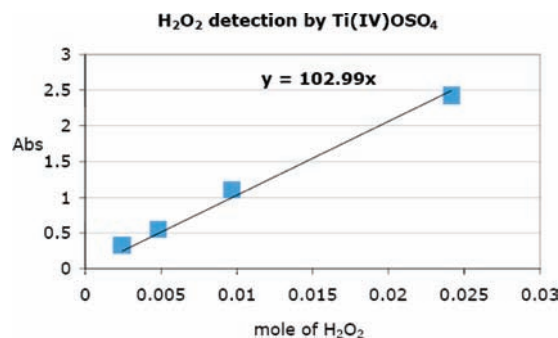
**Synthesis of Cu(I) Complexes and Their Reactivity toward  $\text{O}_2$ .** [ $\text{L}^{\text{MIm}}$ ] $\text{Cu}^{\text{I}}\text{ClO}_4$ .  $\text{L}^{\text{MIm}}$  (0.10 g, 0.37 mmol) and [ $\text{Cu}^{\text{I}}(\text{CH}_3\text{CN})_4\text{ClO}_4$ ] (0.12 g, 0.35 mmol) were dissolved in  $\text{O}_2$ -free  $\text{CH}_3\text{CN}$  (15 mL) in a 50 mL Schlenk flask and stirred for 1 h under Ar at RT. The resulting yellow solution was filtered and transferred by cannula (with filter paper) to a 100 mL Schlenk flask. The complex was precipitated as a yellow powder upon addition of  $\text{O}_2$ -free diethylether. The supernatant was decanted and the resulting yellow powder was washed two times with  $\text{O}_2$ -free diethylether and dried under vacuum to give 0.13 g (0.29 mmol, 83%) of yellow powder product.  $^1\text{H NMR}$  (nitromethane- $d_3$ ):  $\delta$  10.2 (s, 1H), 8.2 (s, 2H), 7.70 (s, 2H), 7.42 (s, 1H), 7.37 (s, 2H), 7.05 (s, 2H), 6.94 (s, 1H), 4.3 (m, 4H), 3.95 (d,  $J = 14.8$  Hz, 2). ESI mass spectrum:  $m/z$  342.31 ( $\text{LCu}^{\text{I}}$ )<sup>+</sup>.<sup>34</sup>

[ $\text{L}^{\text{MIm}}$ ] $\text{Cu}^{\text{I}}\text{B}(\text{C}_6\text{F}_5)_4$ . In a 50 mL Schlenk flask,  $\text{L}^{\text{MIm}}$  (0.29 g, 1.0 mmol) and [ $\text{Cu}^{\text{I}}(\text{CH}_3\text{CN})_4\text{B}(\text{C}_6\text{F}_5)_4$ ] (0.81 g, 0.93 mmol) were dissolved in  $\text{O}_2$ -free THF (15 mL) and stirred for 1 h under Ar at RT. The resulting yellow solution was filtered and transferred by cannula (with filter paper) to a 100 mL Schlenk flask. The complex precipitated as a yellow powder upon addition of  $\text{O}_2$ -free heptane into the reaction mixture. The supernatant was decanted, and the resulting yellow powder (0.85 g, 0.80 mmol, 86%) was washed two times with  $\text{O}_2$ -free pentane and dried under vacuum.  $^1\text{H NMR}$  ( $\text{DMSO}-d_6$ ):  $\delta$  12.5 (s, br, 1H), 7.5 (m, 10H), 4.05 (s, br, 6H), 3.59 (THF), 1.75 (THF), 1.2 (pentane), 0.8 (pentane).<sup>34</sup>

[ $\text{L}^{\text{EIm}}$ ] $\text{Cu}^{\text{I}}\text{B}(\text{C}_6\text{F}_5)_4$ .  $\text{L}^{\text{EIm}}$  (0.40 g, 1.36 mmol) and [ $\text{Cu}^{\text{I}}(\text{CH}_3\text{CN})_4\text{B}(\text{C}_6\text{F}_5)_4$ ] (1.23 g, 1.4 mmol) were dissolved and stirred for 1 h in  $\text{O}_2$ -free THF (15 mL) under Ar at RT. The resulting yellow solution was filtered and transferred to a 100 mL Schlenk flask by cannula (with filter paper). The complex precipitated as a yellow powder upon addition of  $\text{O}_2$ -free heptane into the reaction mixture. The supernatant was decanted, and the resulting yellow powder (1.28 g, 1.2 mmol, 88%) was washed two times with  $\text{O}_2$ -free heptane and dried under vacuum.  $^1\text{H NMR}$  ( $\text{DMSO}-d_6$ ):  $\delta$  12.43 (s, br, 1H), 8.76 (s, 2H), 8.13 (s, 1H), 7.85 (s, 2H), 7.45 (m, 4H), 7.04 (s, 1H), 4.05 (s, br, 4H), 2.75 (s, br, 4H), 1.2 (heptane), 0.8 (heptane). Anal. Calcd for  $\text{C}_{41}\text{H}_{19}\text{BCuF}_{20}\text{N}_5$  ( $1/3\text{C}_7\text{H}_{16}$ ): C, 48.67; H, 2.29; N, 6.55. Found: C, 48.49; H, 2.16; N, 6.40. FAB mass spectrum:  $m/z$  356.3 ( $\text{LCu}^{\text{I}}$ )<sup>+</sup>.

**Tetramer [ $\text{L}^{\text{EIm}^-}$ ] $(\text{Cu}^{\text{II}})_4\text{B}(\text{C}_6\text{F}_5)_4$  Synthesis.** The  $\text{B}(\text{C}_6\text{F}_5)_4$  salt of [ $\text{L}^{\text{EIm}}$ ] $\text{Cu}^{\text{I}}$  (2a) (180 mg, 0.17 mmol) was stirred for 1 h in THF (5 mL) under air at RT. The resulting green solution was layered with diethylether and pentane. After 1–2 days, a green crystalline material was isolated. After this was washed two times with pentane and was vacuum dried, the yield of green crystalline product was 137 mg (0.033 mmol, 78%). UV-vis (MeCN;  $\lambda_{\text{max}}$ , nm;  $\epsilon$ ,  $\text{M}^{-1}\text{cm}^{-1}$ ): 700, 450. Anal. Calcd for  $\text{C}_{166}\text{H}_{76}\text{B}_4\text{Cl}_4\text{Cu}_4\text{F}_{80}\text{N}_{20}$ : C, 46.26; H, 1.78; N, 6.50. Found: C, 46.15; H, 1.58; N, 6.11. X-ray quality green crystals were obtained from the synthesis.

**Detection of Hydrogen Peroxide by  $\text{Ti}(\text{IV})\text{O}(\text{SO}_4)$ .** Hydrogen peroxide produced from the reaction of the peroxo [ $\{(\text{L}^{\text{EIm}})\text{Cu}^{\text{II}}\}_2(\text{O}_2^{2-})\}^{2+}$  (2b<sup>P</sup>) with [ $\text{H}(\text{OEt}_2)_2\text{B}(\text{C}_6\text{F}_5)_4$ ] was determined spectrophotometrically with titanium(IV) oxysulfate.<sup>35,36</sup> The  $\text{B}(\text{C}_6\text{F}_5)_4$  salt of [ $\text{L}^{\text{EIm}}$ ] $\text{Cu}^{\text{I}}$  (2a) (70 mg, 0.066 mmol) was dissolved in  $\text{O}_2$ -free THF (5 mL) in the drybox. The yellow solution turned to a deep blue color corresponding to an end-on peroxo species after bubbling  $\text{O}_2$  gas at  $-94$  °C. After [ $\text{H}(\text{OEt}_2)_2\text{B}(\text{C}_6\text{F}_5)_4$ ] (67 mg, 0.081 mmol) was introduced to the resulting blue solution, distilled water (10 mL) and  $\text{CH}_2\text{Cl}_2$  (20 mL) were added. To the separated aqueous layer, a  $\text{Ti}(\text{IV})\text{O}(\text{SO}_4)$  solution (0.1 mL; titanium(IV) oxysulfate, 15% in sulfuric acid) was introduced. The concentration of the hydrogen peroxide was spectroscopically measured from the absorption at 408 nm (0.96), and the yield was 28%. The calibration curve was derived from the absorption measurements of a 2.416 mM  $\text{H}_2\text{O}_2$  (29.58%, VWR) stock solution. Upon addition of 0.1 mL of a  $\text{Ti}(\text{IV})\text{O}(\text{SO}_4)$  solution to 10 mL of the aqueous solution with varying concentrations of hydrogen peroxide (from stock solution: 1, 2, 4, and 10 mL; 0.00242, 0.00483, 0.00966, and 0.0242 mmol, respectively), the absorption at 408 nm was measured (0.332, 0.553, 1.11, and 2.42, respectively).



Calibration curve of the moles of hydrogen peroxide in aqueous solution with  $\text{Ti}(\text{IV})\text{O}(\text{SO}_4)$ .

(34) Because of the copper(I)– $\text{L}^{\text{MIm}}$  complex extreme air sensitivity, even after many tries we were not able to obtain proper C, H, and N elemental analyses. The expected  $^1\text{H NMR}$  spectra of these complexes and other clean behavior attests to their high purity in terms of the chemistry described in this paper.

(35) Chaudhuri, P.; Hess, M.; Mueller, J.; Hildenbrand, K.; Bill, E.; Weyhermueller, T.; Wieghardt, K. *J. Am. Chem. Soc.* **1999**, *121*, 9599–9610.  
(36) Eisenberg, G. M. *Ind. Eng. Chem., Anal. Ed.* **1943**, *15*, 327–328.

**[H(OEt<sub>2</sub>)<sub>2</sub>][B(C<sub>6</sub>F<sub>5</sub>)<sub>4</sub>]** **Synthesis.** [H(OEt<sub>2</sub>)<sub>2</sub>][B(C<sub>6</sub>F<sub>5</sub>)<sub>4</sub>] was prepared by the literature procedure.<sup>37</sup> Potassium tetrakis(pentafluorophenyl)borate (2.3 g, 3.2 mmol) was dissolved in diethylether (20 mL). Hydrochloric acid in diethylether (6 mL) was introduced under Ar at -77 °C. The reaction mixture was slowly warmed and stirred at RT for 2 h. After filtration with dried Celite 545, the solvent was evaporated leaving ~6–7 mL of solution. The resulting mixture was put in the freezer for 1 h. After the supernatant was decanted, the colorless crystals obtained were dried under vacuum, giving 1.44 g of product (54%).

**Synthesis and Characterization of Cu(II) Complexes.** [(L<sup>MIm</sup>)Cu<sup>II</sup>(CH<sub>3</sub>CN)]<sup>2+</sup> (**1c**). L<sup>MIm</sup> (0.45 g, 1.6 mmol) and Cu<sup>II</sup>(ClO<sub>4</sub>)<sub>2</sub>·6H<sub>2</sub>O (0.59 g, 1.6 mmol) were dissolved in CH<sub>3</sub>CN (15 mL) and stirred for 1 h at room temperature. The resulting blue solution was filtered and transferred to a 100 mL Schlenk flask with a cannula (with filter paper). The solution was layered with diethylether and allowed to stand for 1 h. After the resulting supernatant was decanted, the resulting powder was washed two times with diethylether and dried under vacuum to give 0.88 g of product (1.48 mmol, 95%). UV-vis (CH<sub>3</sub>CN; λ<sub>max</sub>, nm; ε, M<sup>-1</sup> cm<sup>-1</sup>): 880, 200; 660 (shoulder), 55. Anal. Calcd for C<sub>16</sub>H<sub>17</sub>Cl<sub>2</sub>CuN<sub>5</sub>O<sub>8</sub>·<sup>5</sup>/<sub>2</sub>H<sub>2</sub>O: C, 32.75; H, 3.78; N, 11.93. Found: C, 32.55; H, 3.23; N, 11.71. ESI mass spectrum: *m/z* 342.29 (LCu)<sup>+</sup>. An EPR spectrum of **1c** indicates a typical trigonal bipyramidal copper environment: X-band spectrometer (ν = 9.487 GHz) in DMF/toluene (1:1) at 4 K; *g*<sub>||</sub> = 1.99, *A*<sub>||</sub> = 70 G; *g*<sub>⊥</sub> = 2.21, *A*<sub>⊥</sub> = 99 G (See Figure 7). X-ray quality green crystals were obtained from acetonitrile layered with diethylether.

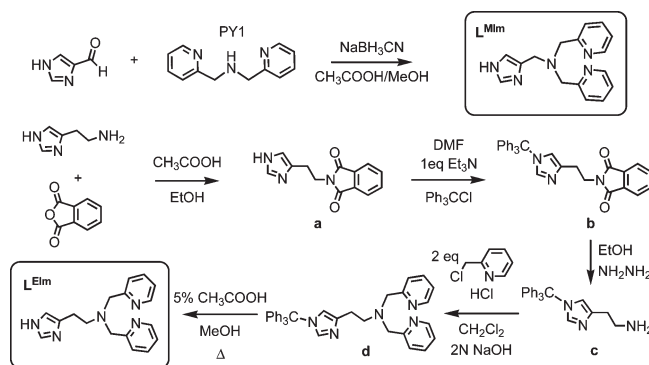
[(L<sup>EIm</sup>)Cu<sup>II</sup>(CH<sub>3</sub>CN)]<sup>2+</sup> (**2c**). L<sup>EIm</sup> (0.50 g, 1.7 mmol) and Cu<sup>II</sup>(ClO<sub>4</sub>)<sub>2</sub>·6H<sub>2</sub>O (0.63 g, 1.7 mmol) were dissolved and stirred for 1 h in CH<sub>3</sub>CN (5 mL) at room temperature. The resulting blue solution was filtered and transferred to a 100 mL Schlenk flask by cannula (with filter paper). The solution was layered with diethyl ether. After the supernatant was decanted, the resulting powder was washed two times with diethyl ether and dried under vacuum to give 0.79 g of product (1.34 mmol, 81%). UV-vis (MeCN; λ<sub>max</sub>, nm; ε, M<sup>-1</sup> cm<sup>-1</sup>): ~300 (shoulder), 2400; 660, 130; ~840, 110. Anal. Calcd for C<sub>17</sub>H<sub>23</sub>Cl<sub>2</sub>CuN<sub>5</sub>O<sub>10</sub>: C, 34.50; H, 3.92; N, 11.83. Found: C, 34.88; H, 3.48; N, 11.32. ESI mass spectrum: *m/z* 356.35 (LCu)<sup>+</sup>. An EPR spectrum of **2c** indicates a typical tetragonal copper environment: X-band spectrometer (ν = 9.488 GHz) in DMF/toluene (1:1) at 4 K; *g*<sub>||</sub> = 2.26, *A*<sub>||</sub> = 161 G; *g*<sub>⊥</sub> = 2.06 (see Figure 7). X-ray quality green crystals were obtained from acetonitrile layered with diethylether.

## Results and Discussion

**Synthesis of Ligands and Copper(I) Complexes.** The imidazolyl containing tetradentate ligands were synthesized by standard methods. L<sup>MIm</sup> was prepared by the reductive coupling reaction of PY1 (dipicolylamine) and 1*H*-imidazole-4-carbaldehyde with sodium cyanoborohydride under acidic conditions, Scheme 2.<sup>38</sup> The L<sup>EIm</sup> synthesis was more involved, but it was successfully prepared according to Scheme 2.

The copper(I) complexes were synthesized by the addition of 1 equiv of the appropriate tripodal ligand to [Cu<sup>I</sup>(CH<sub>3</sub>CN)<sub>4</sub>]Y (Y = ClO<sub>4</sub><sup>-</sup>, B(C<sub>6</sub>F<sub>5</sub>)<sub>4</sub><sup>-</sup>)<sup>30,31</sup> in CH<sub>3</sub>CN or THF under argon. They are both yellow air-sensitive solids. Nujol mull IR spectra reveal absorptions ascribed to the ligand N–H moiety (Experimental Section). We were not able to crystallize either [(L<sup>MIm</sup>)Cu<sup>I</sup>]<sup>+</sup> (**1a**) and

**Scheme 2**



[(L<sup>EIm</sup>)Cu<sup>I</sup>]<sup>+</sup> (**2a**). For ligand–copper(I) complexes with nitrogen containing tri- or tetradentate ligands, a dimeric structure may be possible; there are examples known in the solid state or in solution,<sup>9,29,39</sup> where one N-donor of a given chelate within [(L)Cu<sup>I</sup>]<sub>2</sub><sup>2+</sup> binds to the “other” copper(I) moiety. Normally in more polar or high-dielectric solvents, the dimer “breaks up” to give mononuclear complexes, e.g., [(L)Cu<sup>I</sup>]<sup>+</sup> or [(L)Cu<sup>I</sup>(solvent)]<sup>+</sup>.<sup>9</sup> Solution conductivity measurements can distinguish between a [(L)Cu<sup>I</sup>]<sup>+</sup> or dimer [(L)Cu<sup>I</sup>]<sub>2</sub><sup>2+</sup> formulation,<sup>9,40</sup> and we carried out such measurements in dimethylformamide (DMF) solvent. In fact, 1:1 electrolyte behavior is observed for both **1a** and **2a**, consistent with mononuclear formulations.<sup>32,33</sup> The molar conductivity values for [(TMPA)Cu<sup>I</sup>(CH<sub>3</sub>CN)]<sup>+</sup>, [(L<sup>MIm</sup>)Cu<sup>I</sup>]<sup>+</sup> (**1a**), and [(L<sup>EIm</sup>)Cu<sup>I</sup>]<sup>+</sup> (**2a**) are 47, 49, and 45 Ω<sup>-1</sup> cm<sup>2</sup> mol<sup>-1</sup>, respectively. Such experiments were not carried out in 2-methyltetrahydrofuran (MeTHF) or THF, which were used for the dioxygen reactivity studies described below, since these are not good solvents for conductivity measurements.<sup>32</sup> Thus, binuclear structures for **1a** or **2a** in these solutions cannot entirely be ruled out.

**CO Binding and Electrochemistry of [(L<sup>MIm</sup>)Cu<sup>I</sup>]<sup>+</sup> (**1a**) and [(L<sup>EIm</sup>)Cu<sup>I</sup>]<sup>+</sup> (**2a**).** In order to obtain insights into the solution state structures of copper(I) complexes, as well as to obtain information concerning the relative amount of electron donation to the copper(I) ion as a function of ligand set (i.e., L<sup>MIm</sup> vs L<sup>EIm</sup> vs TMPA), carbon monoxide binding to [(L<sup>MIm</sup>)Cu<sup>I</sup>]<sup>+</sup> (**1a**) and [(L<sup>EIm</sup>)Cu<sup>I</sup>]<sup>+</sup> (**2a**) was examined. The two C–O stretching frequencies at 2090 and 2073 cm<sup>-1</sup> observed for [(TMPA)Cu<sup>I</sup>(CO)]<sup>+</sup> have previously been attributed to a dynamic equilibrium involving overall 4- or 5-coordinate complexes, the former structure possessing an uncoordinated pyridyl arm.<sup>5,41,42</sup> The lower value is ascribed to the pentacoordinate species where ligation of all four N-donors provides more electron density to the Cu(I) ion, resulting in greater back-donation to the CO π\* orbital (thus weakening the CO bond and lowering ν(C–O)). An almost identical behavior is exhibited by [(L<sup>MIm</sup>)Cu<sup>I</sup>]<sup>+</sup> (**1a**), with CO vibrational frequencies at 2087 and 2063 cm<sup>-1</sup>, Table 1

(39) Carrier, S. M.; Ruggiero, C. E.; Houser, R. P.; Tolman, W. B. *Inorg. Chem.* **1993**, *32*, 4889–4899.

(40) Himes, R. A.; Park, G. Y.; Barry, A. N.; Blackburn, N. J.; Karlin, K. D. *J. Am. Chem. Soc.* **2007**, *129*, 5352–5353.

(41) Kretzer, R. M.; Ghiladi, R. A.; Lebeau, E. L.; Liang, H.-C.; Karlin, K. D. *Inorg. Chem.* **2003**, *42*, 3016–3025.

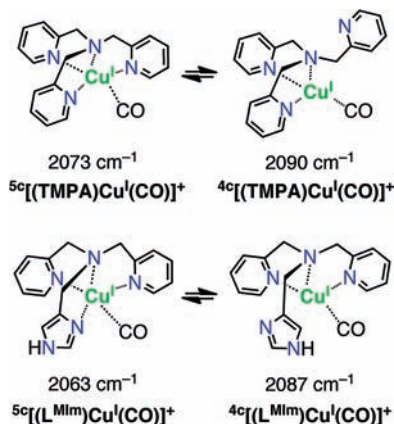
(42) Fry, H. C.; Lucas, H. R.; Narducci Sarjeant, A. A.; Karlin, K. D.; Meyer, G. J. *Inorg. Chem.* **2008**, *47*, 241–256.

(37) Jutzi, P.; Muller, C.; Stammler, A.; Stammler, H. G. *Organometallics* **2000**, *19*, 1442–1444.

(38) Ohtsu, H.; Shimazaki, Y.; Odani, A.; Yamauchi, O.; Mori, W.; Itoh, S.; Fukuzumi, S. *J. Am. Chem. Soc.* **2000**, *122*, 5733–5741.

**Table 1.** Carbonyl Stretching Frequencies for Copper(I) Carbonyl Complexes in THF and Cyclic Voltammetry Data for Cuprous Complexes in DMF

compound	CO (cm <sup>-1</sup> )	E <sub>1/2</sub> <sup>a</sup>
[(TMPA)Cu <sup>I</sup> (CH <sub>3</sub> CN)] <sup>+</sup>	2090, 2073	-610
[(L <sup>MIm</sup> )Cu <sup>I</sup> ] <sup>+</sup> ( <b>1a</b> )	2087, 2063	-620
[(L <sup>EIm</sup> )Cu <sup>I</sup> ] <sup>+</sup> ( <b>2a</b> )	2082	-570

<sup>a</sup> In millivolts (mV) vs Fe(Cp)<sub>2</sub><sup>+0</sup>.**Scheme 3**

and Scheme 3. The five-coordinate isomer of [(L<sup>MIm</sup>)Cu<sup>I</sup>(CO)]<sup>+</sup>, designated **5c**(**1a-CO**), has a lower  $\nu(\text{C-O})$  value (10 cm<sup>-1</sup>) than the corresponding isomer for [(TMPA)Cu<sup>I</sup>(CO)]<sup>+</sup> (2063 vs 2073 cm<sup>-1</sup>, Table 1), indicating that the imidazolyl group in L<sup>MIm</sup> (and L<sup>EIm</sup>, see below) when coordinated to copper(I) is a better donor than is a pyridyl moiety in these tripodal ligands. With these observations, we conclude the putative four-coordinate isomer of L<sup>MIm</sup>, **4c**[(L<sup>MIm</sup>)Cu<sup>I</sup>(CO)]<sup>+</sup> (**1a-CO**) (Scheme 3) does not have its imidazolyl group copper ion bound, since the  $\nu(\text{C-O})$  value is nearly the same as that for the four-coordinate TMPA copper-carbonyl complex (2087 vs 2090 cm<sup>-1</sup>, Table 1). On the other hand, for the L<sup>EIm</sup> complex, only one isomer is observed based on the observation of a single IR absorption (Table 1); the band is 8 cm<sup>-1</sup> lowered from the 2090 cm<sup>-1</sup> value for [(TMPA)Cu<sup>I</sup>(CO)]<sup>+</sup>. Thus, to account for some lowering of  $\nu(\text{C-O})$ , [(L<sup>EIm</sup>)Cu<sup>I</sup>(CO)]<sup>+</sup> (**2a-CO**) could be a four-coordinate species where L<sup>EIm</sup> acts as a tridentate ligand but with the imidazolyl rather than pyridyl group binding. However, we cannot rule out a five-coordinate formulation with all N-donors ligating but where a geometric/coordination effect leads to less back-donation to copper(I) in **5c**[(L<sup>EIm</sup>)Cu<sup>I</sup>(CO)]<sup>+</sup> then observed for [(TMPA)Cu<sup>I</sup>(CO)]<sup>+</sup>.

The electrochemical behavior of [(TMPA)Cu<sup>I</sup>(CH<sub>3</sub>CN)]<sup>+</sup>, [(L<sup>MIm</sup>)Cu<sup>I</sup>]<sup>+</sup> (**1a**) and [(L<sup>EIm</sup>)Cu<sup>I</sup>]<sup>+</sup> (**2a**) was measured by cyclic voltammetry in DMF under Ar; the E<sub>1/2</sub> values obtained (vs Fe(Cp)<sub>2</sub><sup>+0</sup>) are listed in Table 1. We find that the E<sub>1/2</sub> value for **1a** is 10 mV more negative than for the TMPA complex (Table 1), suggesting an effect of better donation from the imidazolyl donor. However, **2a** possesses an E<sub>1/2</sub> value which is 50 mV more positive than **1a**, indicating [(L<sup>MIm</sup>)Cu<sup>I</sup>]<sup>+</sup> (**1a**) is a stronger reductant than **2a**. Redox potentials are affected by factors other than only ligand donation, such as coordi-

nation geometry.<sup>43,44</sup> The relatively high redox potential of [(L<sup>EIm</sup>)Cu<sup>I</sup>]<sup>+</sup> (**2a**) compared to the TMPA complex and [(L<sup>MIm</sup>)Cu<sup>I</sup>]<sup>+</sup> (**1a**) likely reflects geometric changes upon oxidation leading to a (relatively) decreased binding constant between Cu(II) and L<sup>EIm</sup>. Such effects are further clarified by studies on the Cu(II) complexes of L<sup>MIm</sup> and L<sup>EIm</sup>, **1c** and **2c**, described below.

**Preparation and Characterization of Mononuclear LCu(II) Complexes.** In order to better understand the nature of the copper(II) ion coordination in the ligand environments of L<sup>MIm</sup> and L<sup>EIm</sup>, we synthesized copper(II) complexes by addition of 1 equiv of the appropriate tetradentate ligand to Cu<sup>II</sup>(ClO<sub>4</sub>)<sub>2</sub>·6H<sub>2</sub>O in CH<sub>3</sub>CN or CH<sub>3</sub>OH (see Experimental Section) at room temperature. In all cases, diffusion of diethylether allows for the formation of crystalline materials that could be characterized by X-ray crystallography.

**X-ray Structure of Cu(II) Complexes with L<sup>MIm</sup> and L<sup>EIm</sup>.** The X-ray structure of [(L<sup>MIm</sup>)Cu<sup>II</sup>(CH<sub>3</sub>CN)]<sup>2+</sup> (**1c**) as perchlorate salt reveals the coordination geometry to be a slightly distorted trigonal bipyramid ( $\tau = 0.86$ , Figure 1), similar but not identical to a previously reported structure of a very closely related ligand-copper(II) complex differing from L<sup>MIm</sup> only in that the imidazolyl group is N-methylated; this has  $\tau = 0.96$ .<sup>38</sup> For a perfect trigonal bipyramidal (TBP) geometry,  $\tau = 1$  while for a square pyramidal geometry,  $\tau = 0$ .<sup>45</sup> The structure of **1c** is also similar to TMPA or analogue cupric complexes with a different fifth ligand such as CH<sub>3</sub>CN, H<sub>2</sub>O, or Cl<sup>-</sup> ( $\tau = 1 - 0.96$ )<sup>46,47</sup> or O<sub>2</sub><sup>2-</sup> as in [(TMPA)<sub>2</sub>Cu<sup>II</sup>(O<sub>2</sub><sup>2-</sup>)<sup>2+</sup> ( $\tau = 0.86$ ).<sup>5</sup> However, the X-ray structure of [(L<sup>EIm</sup>)Cu<sup>II</sup>(CH<sub>3</sub>CN)(<sup>-</sup>OCIO<sub>3</sub>)]<sup>+</sup> (**2c**·OCIO<sub>3</sub>) (Figure 1) indicates a distortion occurs, with a square pyramidal arrangement of the five N-donors from L<sup>EIm</sup> plus CH<sub>3</sub>CN; the copper ion is displaced 0.13 Å out of the least-squares plane defined by N1, N2, N4, N6, toward the axial N3<sub>pyridyl</sub> ligand and  $\tau = 0.19$  considering only these ligands. There is also a weakly coordinating perchlorate O-atom occupying the other axial position, Figure 1. Thus, one more methylene group (L<sup>EIm</sup> vs L<sup>MIm</sup>) considerably changes the local copper(II) coordination geometry.

In fact, this result is not unexpected, and is already known from studies of a variety of pyridylalkylamine containing five-coordinate cupric complexes with varying chelate ring size.<sup>46,48-50</sup> Thus the additional methylene

(43) Ambundo, E. A.; Deydier, M.-V.; Grall, A. J.; Aguera-Vega, N.; Dressel, L. T.; Cooper, T. H.; Heeg, M. J.; Ochrymowicz, L. A.; Rorabacher, D. B. *Inorg. Chem.* **1999**, *38*, 4233-4242.

(44) Rorabacher, D. B. *Chem. Rev.* **2004**, *104*, 651-697.

(45) Addison, A. W.; Rao, T. N.; Reedijk, J.; van Rijn, J.; Verschoor, G. C. *J. Chem. Soc., Dalton Trans.* **1984**, 1349-1356.

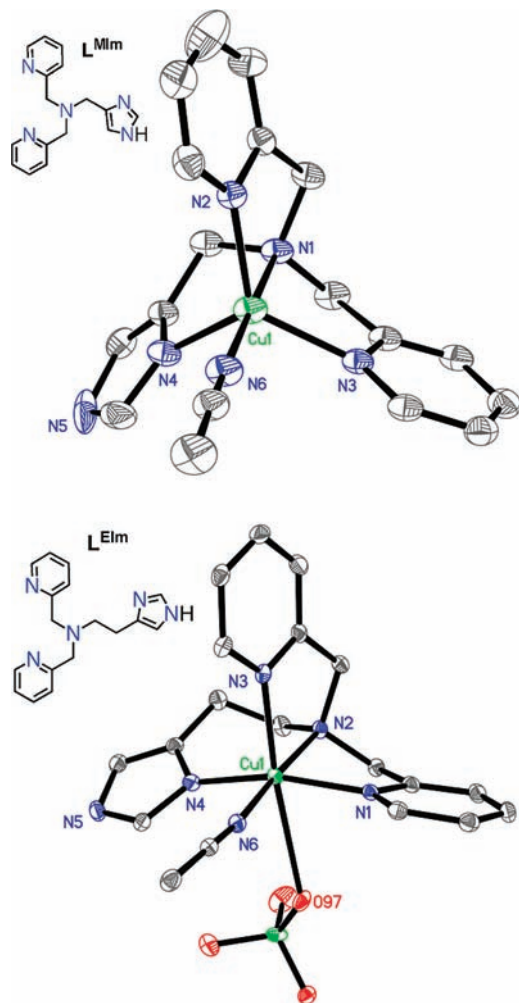
(46) Lucchese, B.; Humphreys, K. J.; Lee, D.-H.; Incarvito, C. D.; Sommer, R. D.; Rheingold, A. L.; Karlin, K. D. *Inorg. Chem.* **2004**, *43*, 5987-5998.

(47) Lim, B. S.; Holm, R. H. *Inorg. Chem.* **1998**, *37*, 4898-4908.

(48) Wei, N.; Murthy, N. N.; Karlin, K. D. *Inorg. Chem.* **1994**, *33*, 6093-6100.

(49) Karlin, K. D.; Hayes, J. C.; Shi, J.; Hutchinson, J. P.; Zubieta, J. *Inorg. Chem.* **1982**, *21*, 4106-4108.

(50) Schatz, M.; Becker, M.; Thaler, F.; Hampel, F.; Schindler, S.; Jacobson, R. R.; Tyeklár, Z.; Murthy, N. N.; Ghosh, P.; Chen, Q.; Zubieta, J.; Karlin, K. D. *Inorg. Chem.* **2001**, *40*, 2312-2322.



**Figure 1.** ORTEP diagram view of the cationic portions of  $[(L^{MIm})Cu^{II}(CH_3CN)]^{2+}$  (**1c**;  $\tau = 0.861$ , top; 30% probability ellipsoids) and  $[(L^{EIm})Cu^{II}(CH_3CN)(^-OClO_3)]^{2+}$  (**2c**;  $^-OClO_3$ , bottom; 30% probability ellipsoids). The hydrogen atoms and noncoordinating perchlorate anions are omitted for clarity.

group on **2c** results in a distortion from TBP to a square pyramidal geometry. As a result of this square pyramidal distortion, the  $N_{imidazole}$  distance in **2c** is shorter than in the TBP **1c** (1.972 vs 2.064 Å) suggesting a stronger Cu(II)–imidazole bond in **2c** than in the TBP **1c**. Further, the axial Cu(1)– $N_{pyridine}$  distance (2.183 Å) is much longer than the other Cu–N distances in **2c**. In both **1c** and **2c**, the Cu(II) ion lies in the plane of the imidazole ring, as shown by the fact that the sum of the angles around the coordinating  $N_{imidazole}$  atom is equal to  $360^\circ$ . In the essentially square pyramidal (without  $ClO_4^-$ , Figure 1)  $[(L^{EIm})Cu^{II}(CH_3CN)]^{2+}$  (**2c**) molecule, the Cu–N–C angles are close to each other (see diagram) and the Cu(II) acceptor orbital has good overlap with the  $N_{imidazole}$  lone-pair orbital, leading to a stronger bond. Other selected bond angles and distances are listed in Table 2.

**Solution Behavior of 1c and 2c:** Electron Paramagnetic Resonance Spectroscopy. In fact, the solid state structures and difference in coordination geometries described above for of  $[(L^{MIm})Cu^{II}(CH_3CN)]^{2+}$  (**1c**) and  $[(L^{EIm})Cu^{II}(CH_3CN)]^{2+}$  (**2c**) are maintained in solution (Note, the perchlorate ion is unlikely to be coordinating in

solution.) EPR spectroscopic data (Figure 2) provide compelling support.  $[(L^{MIm})Cu^{II}(CH_3CN)]^{2+}$  (**1c**) exhibits a “reverse” axial EPR spectrum ( $g_{\parallel} = 1.99$ ,  $A_{\parallel} = 70$  G;  $g_{\perp} = 2.21$ ,  $A_{\perp} = 99$  G), which is indicative of a system with a  $d_{z^2}$  ground state ( $g_{\perp} > g_{\parallel} \sim 2$  and  $A_{\perp} = 60\text{--}100 \times 10^{-4} \text{ cm}^{-1}$ )<sup>46,49,51,52</sup> and thus TBP geometry. On the other hand, the EPR spectrum of  $[(L^{EIm})Cu^{II}(CH_3CN)]^{2+}$  (**2c**) ( $g_{\parallel} = 2.26$ ,  $A_{\parallel} = 161$  G;  $g_{\perp} = 2.06$ ) shows a typical square based pyramidal (tetragonal) copper(II) environment, which is a system with a  $d_{x^2-y^2}$  ground state revealing a regular axial (tetragonal) EPR signature ( $g_{\parallel} > 2.1 > g_{\perp} > 2.0$  and  $A_{\parallel} = 158\text{--}200 \times 10^{-4} \text{ cm}^{-1}$ ).<sup>46,48,53</sup>

**Low-Temperature Formation of Copper–Dioxygen Adducts: End-on Peroxo Dicopper(II) Complex Formation with  $[(L^{MIm})Cu^I]^+$  (**1a**) and  $[(L^{EIm})Cu^I]^+$  (**2a**).** In the past few years we have found that going to relatively nonpolar solvents such as THF, MeTHF, or even  $Et_2O$  and toluene leads to new ligand–Cu(I)/ $O_2$  chemistry and insights. For these purposes, copper(I) complexes as  $B(C_6F_5)_4^-$  salts are employed. When yellow MeTHF solutions of  $[(L^{MIm})Cu^I]^+$  (**1a**) ( $\lambda_{max} = 350$  nm (sh);  $\epsilon \sim 1500 \text{ M}^{-1} \text{ cm}^{-1}$ ) or  $[(L^{EIm})Cu^I]^+$  (**2a**) ( $\lambda_{max} = 337$  nm;  $\epsilon \sim 4100 \text{ M}^{-1} \text{ cm}^{-1}$ ) are oxygenated at  $-128^\circ\text{C}$ , intensely purple-colored solutions form, each having the characteristic spectrum of an end-on  $\mu$ -1,2-peroxo-dicopper(II) complex (Scheme 4), with three prominent LMCT bands, with most intense coming at 525–540 nm accompanied by a lower energy transition or shoulder at 600–610 nm, see Figures 3 and 4 and Table 3. The position of the absorptions for  $[(L^{MIm})Cu^{II}]_2(O_2^{2-})^{2+}$  (**1b<sup>P</sup>**) and  $[(L^{EIm})Cu^{II}]_2(O_2^{2-})^{2+}$  (**2b<sup>P</sup>**) compare closely to that known for the “parent” compound  $[(TMPA)Cu^{II}]_2(O_2^{2-})^{2+}$ .<sup>2,4–6</sup> The absorptivity of the three LMCT absorptions for **2b<sup>P</sup>** match very well to those for  $[(TMPA)Cu^{II}]_2(O_2^{2-})^{2+}$ , however those for **1b<sup>P</sup>** are about one-third lower in intensity (Figure 5 and Table 3). We thus conclude that at  $-128^\circ\text{C}$ , the peroxo–dicopper(II) dioxygen adduct **2b<sup>P</sup>** is essentially fully formed, while the reaction of **1a** with  $O_2$  does not go to completion. Consistent with this is the finding that the **1a**/ $O_2$  reaction is not even observed at  $-80^\circ\text{C}$  in THF; the binding under these conditions is too weak, probably for entropic reasons (by comparison to the  $O_2$  reactions with **2a** or  $[(TMPA)Cu^I(CH_3CN)]^+$ ). The oxygenation of **2a** occurs very rapidly, even at  $-128^\circ\text{C}$ .<sup>54</sup> See Table 3, which summarizes all the spectroscopic data for the complexes with  $L^{MIm}$  and  $L^{EIm}$  in comparison with other copper–dioxygen complexes with tripodal tetradentate ligands.

**Absorption Spectra of 1b<sup>P</sup> and 2b<sup>P</sup>.** While the absorption spectrum of  $[(L^{MIm})Cu^{II}]_2(O_2^{2-})^{2+}$  (**1b<sup>P</sup>**) shows similar charge transfer energies compared to  $[(TMPA)Cu^{II}]_2(\mu$ -1,2- $O_2^{2-})^{2+}$ , the absorption spectrum of  $[(L^{EIm})Cu^{II}]_2(O_2^{2-})^{2+}$  (**2b<sup>P</sup>**) reveals a significant red shift (15 nm)

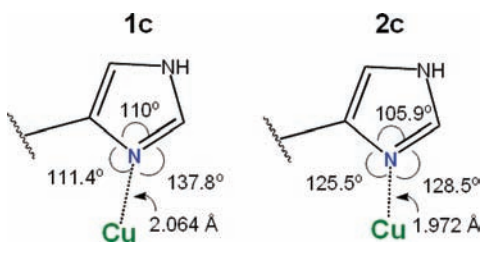
(51) Barbucci, R.; Bencini, A.; Gatteschi, D. *Inorg. Chem.* **1977**, *16*, 2117.

(52) Jiang, F.; Karlin, K. D.; Peisach, J. *Inorg. Chem.* **1993**, *32*, 2576–2582.

(53) Wei, N.; Murthy, N. N.; Chen, Q.; Zubieta, J.; Karlin, K. D. *Inorg. Chem.* **1994**, *33*, 1953–1965.

(54) Both **1b<sup>P</sup>** and **2b<sup>P</sup>** are stable at  $-128^\circ\text{C}$  for more than an hour and qualitatively have generally similar stability compared to  $[(TMPA)Cu^{II}]_2(O_2^{2-})^{2+}$ , based on observable thermal decomposition times as measured by absorbance loss.

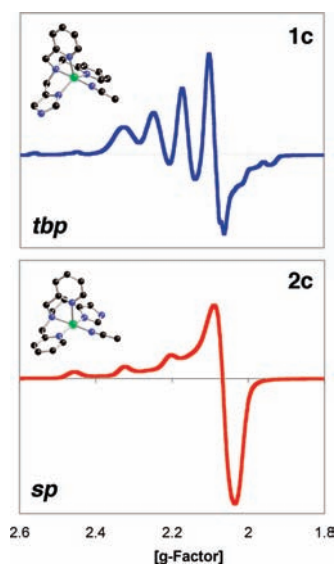


**Table 2.** Selected Bond Distances and Angles for **1c** and **2c·OCIO<sub>3</sub>**


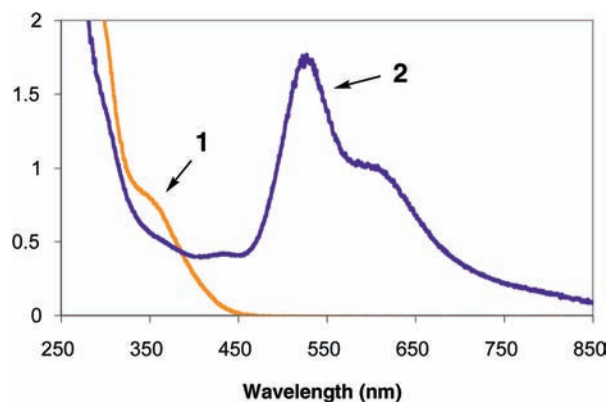
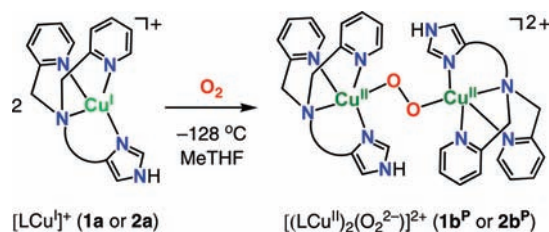
[(L <sup>MIm</sup> )Cu <sup>II</sup> (CH <sub>3</sub> CN)] <sup>2+</sup> ( <b>1c</b> )		[(L <sup>EIm</sup> )Cu <sup>II</sup> (CH <sub>3</sub> CN)( <sup>-</sup> OCIO <sub>3</sub> )] <sup>+</sup> ( <b>2c·OCIO<sub>3</sub></b> )	
Cu–N	bond distance (Å)	Cu–N	bond distance (Å)
Cu(1)–N(1)	2.037(3)	Cu(1)–N(1)	2.005(3)
Cu(1)–N(2)	2.035(3)	Cu(1)–N(2)	2.090(3)
Cu(1)–N(3)	2.039(3)	Cu(1)–N(3)	2.183(3)
Cu(1)–N(4)	2.064(4)	Cu(1)–N(4)	1.972(3)
Cu(1)–N(6)	1.969(3)	Cu(1)–N(6)	2.014(3)
		Cu(1)–O(97)	2.770(9)

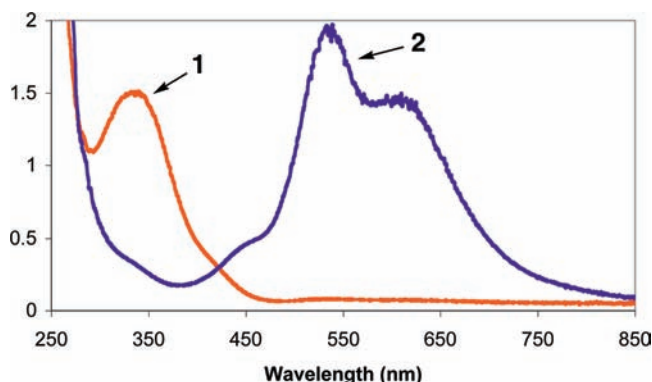
[(L <sup>MIm</sup> )Cu <sup>II</sup> (CH <sub>3</sub> CN)] <sup>2+</sup> ( <b>1c</b> )		[(L <sup>EIm</sup> )Cu <sup>II</sup> (CH <sub>3</sub> CN)( <sup>-</sup> OCIO <sub>3</sub> )] <sup>+</sup> ( <b>2c·OCIO<sub>3</sub></b> )	
N–Cu–N	bond angle (deg)	N–Cu–N	bond angle (deg)
N(6)–Cu(1)–N(2)	96.19(13)	N(4)–Cu(1)–N(1)	161.92(11)
N(6)–Cu(1)–N(1)	177.60(16)	N(4)–Cu(1)–N(6)	91.52(10)
N(2)–Cu(1)–N(1)	82.16(12)	N(1)–Cu(1)–N(6)	93.51(11)
N(6)–Cu(1)–N(3)	96.69(13)	N(4)–Cu(1)–N(2)	94.98(11)
N(2)–Cu(1)–N(3)	125.94(13)	N(1)–Cu(1)–N(2)	80.63(10)
N(1)–Cu(1)–N(3)	82.93(13)	N(6)–Cu(1)–N(2)	173.39(10)
N(6)–Cu(1)–N(4)	99.87(14)	N(4)–Cu(1)–N(3)	97.07(10)
N(2)–Cu(1)–N(4)	116.08(13)	N(1)–Cu(1)–N(3)	99.57(10)
N(1)–Cu(1)–N(4)	82.44(13)	N(6)–Cu(1)–N(3)	96.70(10)
N(3)–Cu(1)–N(4)	112.92(14)	N(2)–Cu(1)–N(3)	81.38(10)

**Figure 2.** EPR spectra of [(L<sup>MIm</sup>)Cu<sup>II</sup>(CH<sub>3</sub>CN)]<sup>2+</sup> (**1c**) (top) and [(L<sup>EIm</sup>)Cu<sup>II</sup>(CH<sub>3</sub>CN)]<sup>2+</sup> (**2c**) (bottom); X-band spectrometer,  $\nu = 9.49$  GHz, in DMF/toluene (1:1) at 4 K. **1c**:  $g_{||} = 1.99$ ,  $A_{||} = 70$  G;  $g_{\perp} = 2.21$ ,  $A_{\perp} = 99$  G. **2c**:  $g_{||} = 2.26$ ,  $A_{||} = 161$  G;  $g_{\perp} = 2.06$ . See text for discussion.

in the dominant  $O_2^{2-}(\pi^*_{\sigma}) \rightarrow Cu(d_{\sigma})$  charge transfer, Table 3 and Figure 5. The relevant absorption for [(TPMA)Cu<sup>II</sup>]<sub>2</sub>( $\mu$ -1,2- $O_2^{2-}$ )<sup>2+</sup> as measured in the present work in MeTHF at  $-128$  °C is  $\lambda_{max} = 520$ ,<sup>55</sup> while for **2b<sup>P</sup>**  $\lambda_{max} = 535$  nm (Figures 4 and 5). As suggested by the

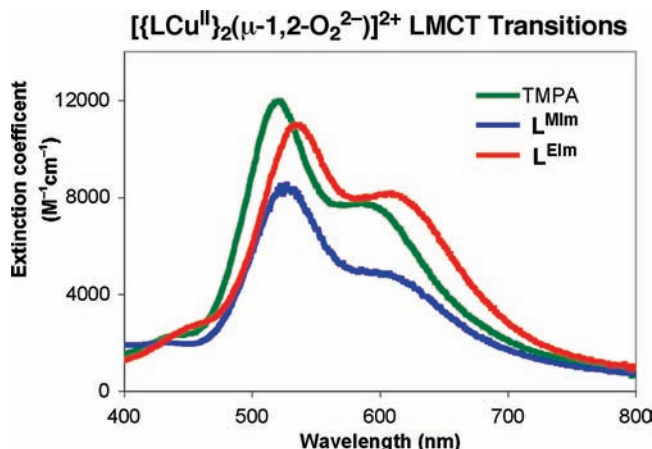
**Figure 3.** Low-temperature UV–vis spectra of the oxygenation of [(L<sup>MIm</sup>)Cu<sup>I</sup>]<sup>+</sup> (**1a**). Spectrum 1: **1a** with absorption at 350 nm ( $1500$  M<sup>-1</sup> cm<sup>-1</sup>). Spectrum 2: [(L<sup>MIm</sup>)Cu<sup>II</sup>]<sub>2</sub>( $O_2^{2-}$ )<sup>2+</sup> (**1b<sup>P</sup>**) with absorption at 435 ( $1700$  M<sup>-1</sup> cm<sup>-1</sup>), 528 ( $6800$  M<sup>-1</sup> cm<sup>-1</sup>), and 605 nm ( $4000$  M<sup>-1</sup> cm<sup>-1</sup>) in MeTHF at  $-128$  °C.**Scheme 4**

X-structure of  $[(L^{EIm})Cu^{II}(CH_3CN)]^{2+}$  (**2c**), the Cu(II) ion in peroxo complex **2b<sup>P</sup>** is expected to be square-pyramidally distorted, due to the geometry of the  $L^{EIm}$  ligand. Thus, the half-occupied Cu  $d_{x^2-y^2}$  orbital of **2b<sup>P</sup>** would be at higher energy than the acceptor  $d_{z^2}$  orbital of the TBP  $[(TMPA)Cu^{II}]_2(\mu-1,2-O_2^{2-})^{2+}$ , based on ligand field differences which, by itself, would blue shift the  $O_2^{2-}(\pi^*_o) \rightarrow Cu(d_o)$  charge transfer. Instead, a red shift of the charge transfer is observed for **2b<sup>P</sup>** compared to  $[(TMPA)Cu^{II}]_2(\mu-1,2-O_2^{2-})^{2+}$ , which reflects the increased electron density in the donor peroxo  $\pi^*_o$ , considerably raising the energy of this donor orbital, resulting in a red shift the  $O_2^{2-}(\pi^*_o) \rightarrow Cu(d_o)$  charge transfer.



**Figure 4.** Low-temperature UV-vis spectra of the oxygenation of  $[(L^{EIm})Cu^I]^+$  (**2a**). Spectrum 1: **2a** with absorption at 337 nm ( $4100 M^{-1} cm^{-1}$ ). Spectrum 2:  $[(L^{EIm})Cu^{II}]_2(O_2^{2-})^{2+}$  (**2b<sup>P</sup>**) with absorption at 445 ( $2500 M^{-1} cm^{-1}$ ), 534 ( $11000 M^{-1} cm^{-1}$ ), and 619 nm ( $8100 M^{-1} cm^{-1}$ ) in MeTHF at  $-128^\circ C$ .

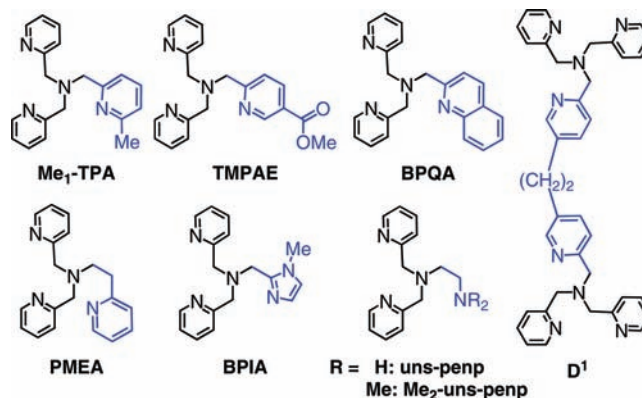
**Resonance Raman Spectroscopy.** The resonance Raman spectrum of  $[(L^{EIm})Cu^{II}]_2(O_2^{2-})^{2+}$  (**2b<sup>P</sup>**) in THF with  $\lambda_{ex} = 568$  nm shows dominant features at 827, 811, and  $539 cm^{-1}$ , which shift to 776 and  $513 cm^{-1}$  upon  $^{18}O_2$  substitution (Figure 6). The 827 and  $811 cm^{-1}$  features are at energies consistent with those of peroxo  $\nu(O-O)$  stretches.<sup>1,2,13</sup> Upon  $^{18}O_2$  substitution, a single  $\nu(O-O)$  is observed at  $776 cm^{-1}$  at higher intensity than either the 827 or  $811 cm^{-1}$  feature. As such, the 827 and  $811 cm^{-1}$  features are assigned as the result of a Fermi resonance of  $\nu(O-O)$  with a local nonenhanced mode of the same symmetry. The preinteraction  $\nu(O-O)$  is estimated to be



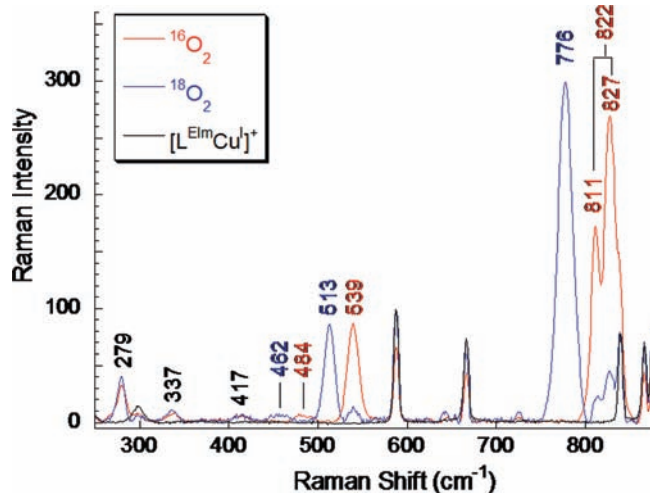
**Figure 5.** UV-visible spectra of  $\mu-1,2$ -peroxo intermediates from  $LCu^I$  complexes ( $L = TMPA, L^{MIm},$  and  $L^{EIm}$ ) reacting with dioxygen at reduced temperature. The  $\epsilon$  value scale for the  $L^{MIm}$  peroxo complex spectrum shown here is not to scale ( $\epsilon_{apparent}$  values are much lower, see text), but shown here in order to easily compare  $\lambda_{max}$  values.

**Table 3.** End-On Peroxo Species with PY1 Based Tetradentate Ligands

	LMCT; nm ( $M^{-1} cm^{-1}$ )			solvent, temp	$\nu(O-O); \Delta(^{18}O_2); cm^{-1}$
TMPA <sup>6</sup>	440 (1700)	525 (11300)	615 (5800)	EtCN, $-80^\circ C$	832; $-44^a$
TMPA <sup>55</sup>	430 (2100)	520 (12000)	590 (8000)	MeTHF, $-128^\circ C$	
$L^{MIm}$	435 (1700)	528 (6800)	605 (4000)	MeTHF, $-128^\circ C$	
$L^{EIm}$	445 (2500)	535 (11000)	610 (8100)	MeTHF, $-128^\circ C$	822; $-46^b$
$D^{160}$	450 (1100)	540 (11100)	600 (8700)	EtCN, $-90^\circ C$	
TMPAE <sup>60</sup>	445 (2000)	532 (9380)	590 (7000)	EtCN, $-80^\circ C$	
$Me_2$ -uns-penp <sup>61</sup>		528 (-)		EtCN, $-90^\circ C$	
uns-penp <sup>62</sup>		535 (-)		acetone, $-90^\circ C$	
BPIA <sup>29</sup>	440 (2000)	535 (11500)	600 (7600)	EtCN, $-80^\circ C$	
BPQA <sup>63</sup>		535 (8600)	600 ( $\sim 6000$ )	EtCN, $-80^\circ C$	
PMEA <sup>64</sup>		536 ( $\sim 5000$ )		EtCN, $-90^\circ C$	
$Me_1$ -TPA <sup>65</sup>	440 (-)	537 ( $\sim 5000$ )	610 (-)	acetone, $-70^\circ C$	
others <sup>2,13</sup>		$\sim 500$	$\sim 600$		812–847



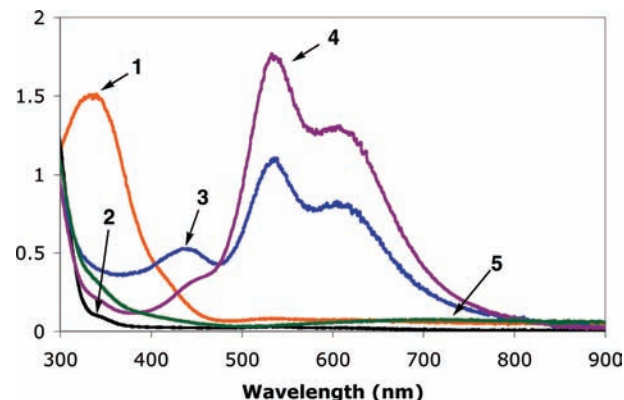
<sup>a</sup> In  $CH_2Cl_2$ . <sup>b</sup> In THF.



**Figure 6.** rR spectra of  $[(L^{EIm})Cu^{II}]_2(O_2^{2-})^{2+}$  ( $2b^P$ ) in THF at 77 K (the red spectrum denotes  $^{16}O_2$ , the blue spectrum denotes  $^{18}O_2$ , and the black spectrum is preoxygenation).  $\lambda_{ex} = 568$  nm.

at  $822\text{ cm}^{-1}$ .<sup>56</sup> The feature at  $539\text{ cm}^{-1}$  ( $\Delta(^{18}O_2) = -26$ ) is assigned as a symmetric  $\nu(\text{Cu}-\text{O})$  stretch based on energy and  $^{18}O_2$ -isotopic shift. These observed vibrations formulate  $2b^P$  as an end-on bound  $\mu$ -1,2 peroxo-dicopper(II) complex.<sup>6</sup> The antisymmetric  $\nu(\text{Cu}-\text{O})$  is observed as a weak, broad feature at  $484\text{ cm}^{-1}$  ( $\Delta(^{18}O_2) = -26$ ). Additional isotope-insensitive features are observed at 417, 337, and  $279\text{ cm}^{-1}$  and are assigned as  $\text{Cu}-N_{\text{pyridine}}$ , internal TPA ring mode, and  $\text{Cu}-N_{\text{imidazole}}$  stretches, respectively.

The O–O stretching frequency of  $2b^P$  is lower (by  $10\text{ cm}^{-1}$ ) than observed for  $[(\text{TPMA})Cu^{II}]_2(O_2^{2-})^{2+}$  ( $832\text{ cm}^{-1}$ ), indicating that  $2b^P$  has a weaker O–O bond. The symmetric Cu–O stretch is also lower than for  $[(\text{TPMA})Cu^{II}]_2(O_2^{2-})^{2+}$  (by  $23\text{ cm}^{-1}$ ), reflecting a weaker Cu–O bond  $2b^P$ .<sup>6</sup> Complex  $2b^P$  is likely distorted from TBP to a more square-pyramidal geometry (as was observed for  $2c$ , vide supra), resulting in better overlap between the ligand N's and Cu's  $d_{x^2-y^2}$  orbital. The high intensity of the  $\text{Cu}-N_{\text{imidazole}}$  vibration in the rR spec-



**Figure 7.** Low-temperature UV-vis spectra in MeTHF at  $-128\text{ }^\circ\text{C}$ . Spectrum 1:  $2a$  with absorption at  $337\text{ nm}$  ( $4\,100\text{ M}^{-1}\text{ cm}^{-1}$ ). Spectrum 2:  $[(L^{EIm})Cu^I(\text{CO})]^+$  without excess CO. Spectrum 3: partial formation of superoxo species  $[(L^{EIm})Cu^{II}(O_2^{\bullet-})]^+$  ( $2b^S$ ) with absorption at  $440\text{ nm}$  and the peroxo complex  $2b^P$ . Spectrum 4:  $2b^P$  with absorption at  $445$  ( $2\,500\text{ M}^{-1}\text{ cm}^{-1}$ ),  $535$  ( $11\,000\text{ M}^{-1}\text{ cm}^{-1}$ ), and  $610\text{ nm}$  ( $8\,100\text{ M}^{-1}\text{ cm}^{-1}$ ). Spectrum 5: thermal decomposition product.

trum ( $279\text{ cm}^{-1}$ , Figure 6) is consistent with an orientation of the lobes of the Cu  $d_{x^2-y^2}$  orbital along the  $\text{Cu}-N_{\text{imidazole}}$  bond. The peroxo  $\pi_{\sigma}^*$  to Cu charge transfer into  $d_{x^2-y^2}$  would result in elongation of the  $\text{Cu}-N_{\text{imidazole}}$  bond and thus its rR enhancement. The square pyramidal environment of each Cu eliminates the inversion center of the dimer, allowing for enhancement of the antisymmetric Cu–O stretch in the rR ( $484\text{ cm}^{-1}$  ( $\Delta(^{18}O_2) = -26$ ), Figure 6). Better orientation of the  $N_{\text{imidazole}}$  ligand lone pair along the lobe of Cu's  $d_{x^2-y^2}$  orbital would facilitate its donation thus reducing donation from the peroxo to the Cu, weakening the Cu–O bond. This decreased peroxo  $\pi_{\sigma}^*$  donation also results in more electron density in the antibonding peroxo  $\pi_{\sigma}^*$  orbital and thus a weaker O–O bond.<sup>57</sup>

**Detection of a Superoxo–Copper(II) Complex with the  $L^{EIm}$  Ligand Complex.** We have been able to detect the initial  $O_2$  adduct arising from dioxygen reactivity in the  $[(L^{EIm})Cu^I]^+$  ( $2a$ ) chemistry. This was accomplished in one manner by first bubbling a  $-128\text{ }^\circ\text{C}$  solution of  $2a$  in MeTHF with carbon monoxide, which gives the colorless CO adduct  $[(L^{EIm})Cu^I(\text{CO})]^+$  (vide supra); the MLCT band at  $337\text{ nm}$  (spectra 1 and 2 in Figure 7) disappears. After elimination of excess CO by vacuum-purging, oxygenation of this solution leads to formation of  $O_2$  adducts, a mixture of the peroxodicopper(II) species  $2b^P$ , and a new absorption near  $440\text{ nm}$  is assigned as the superoxo complex  $[(L^{EIm})Cu^{II}(O_2^{\bullet-})]^+$  ( $2b^S$ ). We have previously used this “trick” of oxygenation of a solution of the carbonyl complex in order to stabilize  $[(\text{Me}_2\text{N-TMPA})Cu^{II}(O_2^{\bullet-})]^+$ .<sup>11</sup> Additional  $O_2$ -bubbling leads to full formation of the peroxo adduct, spectrum 4 in Figure 7.

A more direct detection of  $[(L^{EIm})Cu^{II}(O_2^{\bullet-})]^+$  ( $2b^S$ ) was possible using a stopped-flow kinetics instrument with diode array full spectrum monitoring. As has been previously extensively studied for oxygenation of  $[(\text{TPMA})Cu^I(\text{CH}_3\text{CN})]^+$  and study of the transient superoxo complex  $[(\text{TPMA})Cu^{II}(O_2^{\bullet-})]^+$ ,<sup>7,9</sup> millisecond mixing of  $[(L^{EIm})Cu^I]^+$  ( $2a$ ) and dioxygen in THF at  $-90\text{ }^\circ\text{C}$  readily reveals the formation of  $2b^S$ , with strong absorption at  $431\text{ nm}$ .<sup>58</sup> The spectroscopic behavior

(55) Unpublished observations.

(56) Skulan, A. J.; Hanson, M. A.; Hsu, H.-f.; Que, L., Jr.; Solomon, E. I. *J. Am. Chem. Soc.* **2003**, *125*, 7344–7356.

(57) A resonance Raman study on  $[(L^{MIm})Cu^{II}]_2(O_2^{2-})^{2+}$  ( $1b^P$ ) was not carried out in the context of this report but will be described in a separate publication.

(58) Species  $2b^S$  has an absorption near  $440\text{ nm}$  in MeTHF solvent. We surmise that this difference compared to in THF solvent may be attributed to a solvent dependence: For  $[(\text{TPMA})Cu^{II}(O_2^{\bullet-})]^+$ , the related absorption occurs at  $410\text{ nm}$  in EtCN but  $425\text{ nm}$  in THF, see ref 10. Further studies are needed to understand these observations.

(59) Paul, P. P.; Tyeklár, Z.; Jacobson, R. R.; Karlin, K. D. *J. Am. Chem. Soc.* **1991**, *113*, 5322–5332.

(60) Lee, D.-H.; Wei, N.; Murthy, N. N.; Tyeklár, Z.; Karlin, K. D.; Kaderli, S.; Jung, B.; Zuberbühler, A. D. *J. Am. Chem. Soc.* **1995**, *117*, 12498–12513.

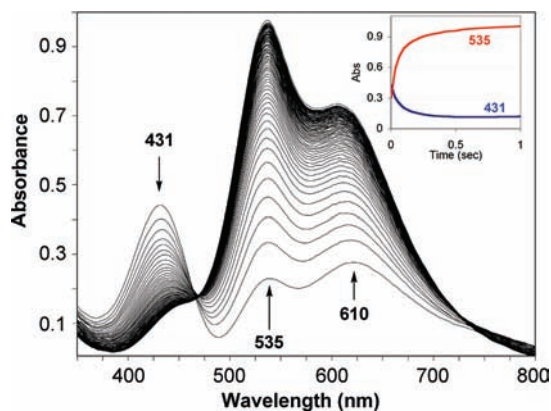
(61) Weitzer, M.; Schatz, M.; Hampel, F.; Heinemann, F. W.; Schindler, S. *J. Chem. Soc. Dalton Trans.* **2002**, 686–694.

(62) Schatz, M.; Leibold, M.; Foxon, S. P.; Weitzer, M.; Heinemann, F. W.; Hampel, F.; Walter, O.; Schindler, S. *Dalton Trans.* **2003**, 1480–1487.

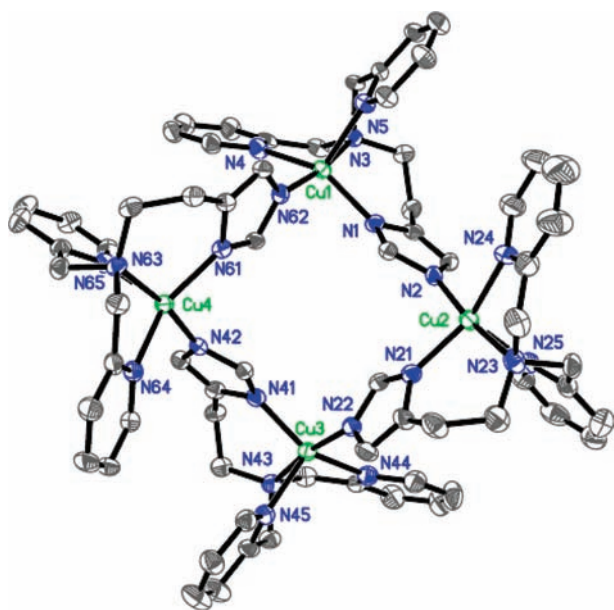
(63) Karlin, K. D.; Wei, N.; Jung, B.; Kaderli, S.; Niklaus, P.; Zuberbühler, A. D. *J. Am. Chem. Soc.* **1993**, *115*, 9506–9514.

(64) Schatz, M.; Becker, M.; Thaler, F.; Hampel, F.; Schindler, S.; Jacobson, R. R.; Tyeklár, Z.; Murthy, N. N.; Ghosh, P.; Chen, Q.; Zubieta, J.; Karlin, K. D. *Inorg. Chem.* **2001**, *40*, 2312–2322.

(65) Uozumi, K.; Hayashi, Y.; Suzuki, M.; Uehara, A. *Chem. Lett.* **1993**, 963–966.



**Figure 8.** Time-dependent UV–visible spectra for the oxygenation of  $[(L^{EIm})Cu^I]^+$  (**2a**) in THF at  $-90\text{ }^\circ\text{C}$  as measured using a stopped-flow kinetics instrument. The inset shows the time dependence of the disappearance of the superoxo complex  $[(L^{EIm})Cu^{II}(O_2^{\cdot-})]^+$  (**2b<sup>S</sup>**) (431 nm) and the corresponding formation of the peroxo complex  $[(L^{EIm})Cu^{II}]_2(O_2^{2-})^{2+}$  (**2b<sup>P</sup>**) monitored at 535 nm. See text for further explanation and discussion.



**Figure 9.** ORTEP view (50% probability ellipsoids) of a tetramer  $[(\mu_2-L^{EIm-})_4(Cu^{II})_4]^{4+}$  cluster (average  $\tau = \sim 0.41$ ). The hydrogen atoms and perchlorate anions are omitted for clarity.

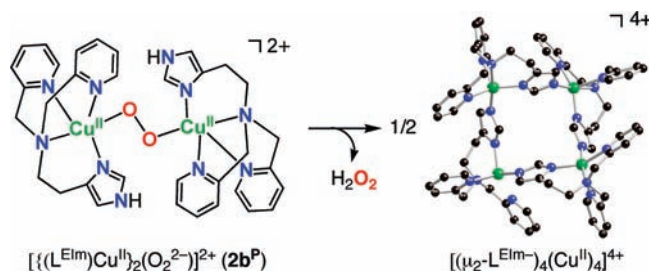
observed in this experiment (Figure 8) reveals that **2b<sup>S</sup>** forms within the instrument mixing time (1–2 ms), as the 431 nm absorption is already decreasing in the first few spectra observed. Thus, from the absorptivity observed here, we conclude that  $\epsilon > 2\,600\text{ M}^{-1}\text{ cm}^{-1}$  at 431 nm for **2b<sup>S</sup>**. At this time, a full stopped-flow kinetic analysis has not been carried out for the **2a**/ $O_2$  reaction chemistry. This will be the subject of future study on a series of copper(I) complexes with tripodal tetradentate ligands varying in donor atoms. Closely related to this will be studies of copper(I)–carbonyl complexes **1a-CO** and **2a-CO** in “flash-and-trap” experiments,<sup>10</sup> to deduce the kinetics of formation of superoxo adducts.

**Tetramer Cluster Formation.** The thermal decomposition product of  $[(L^{EIm})Cu^{II}]_2(O_2^{2-})^{2+}$  (**2b<sup>P</sup>**), following warming  $-80\text{ }^\circ\text{C}$  solutions in THF, is a green crystalline material obtained in high yield. X-ray structural analysis

**Table 4.** Selected Bond Distances of a Tetramer  $[(\mu_2-L^{EIm-})_4(Cu^{II})_4]^{4+}$  Cluster

Cu–N	bond distance (Å)	Cu–N	bond distance (Å)
Cu(1)–N(62)	1.967(3)	Cu(3)–N(41)	1.969(4)
Cu(1)–N(1)	1.984(4)	Cu(3)–N(22)	1.973(4)
Cu(1)–N(4)	2.046(4)	Cu(3)–N(44)	2.027(4)
Cu(1)–N(3)	2.090(3)	Cu(3)–N(43)	2.098(4)
Cu(1)–N(5)	2.197(4)	Cu(3)–N(45)	2.185(4)
Cu(2)–N(2)	1.957(4)	Cu(4)–N(42)	1.963(3)
Cu(2)–N(21)	1.967(4)	Cu(4)–N(61)	1.978(4)
Cu(2)–N(24)	2.046(4)	Cu(4)–N(64)	2.039(4)
Cu(2)–N(23)	2.095(4)	Cu(4)–N(63)	2.089(3)
Cu(2)–N(25)	2.222(4)	Cu(4)–N(65)	2.187(4)

**Scheme 5**



identified it as a tetranuclear  $[(\mu_2-L^{EIm-})_4(Cu^{II})_4]^{4+}$  cluster, Figure 9. It is constructed from four cupric ions and four anionic (i.e., with deprotonated imidazolyl)  $L^{EIm-}$  ligands. Each copper center has a distorted square pyramidal geometry with an average  $\tau = 0.41$  ( $\tau = 0.0$  for a perfect square pyramid (SP), vide supra). Supporting the arguments made above, this is another example of a copper complex in the  $L^{EIm}$  framework which prefers a (distorted) SP rather than a TBP coordination geometry. The average  $Cu \cdots Cu$  distance in the cluster is 5.877 Å. Other selected Cu–N bonds are listed in Table 4. The presence of the anionic imidazolate group here suggested to us the probability that hydrogen peroxide was generated during decomposition of **2b<sup>P</sup>**, Scheme 5, with the imidazolyl N–H given up to form  $H_2O_2$ . We tried to test for this possibility using the titanium(IV) oxysulfate reagent to interrogate the warmed up solution of **2b<sup>P</sup>**; this should give an optical change at 408 nm when it reacts with  $H_2O_2$  (see Experimental Section).<sup>35,36</sup> However, no  $H_2O_2$  was detected, perhaps due to metal complex mediated disproportionation chemistry or oxidation of solvent (which we did not probe). Hydrogen peroxide was produced in 28% yield when  $[H(OEt_2)_2][B(C_6F_5)_4]$  was added to the peroxo species **2b<sup>P</sup>** at  $-94\text{ }^\circ\text{C}$ , warming and workup. Such a result (but in better yield) occurs when  $[(TMPA)Cu^{II}]_2(O_2^{2-})^{2+}$  is protonated with mineral acids or even phenols.<sup>59</sup> In fact, the thermal decomposition of  $[(L^{MIm})Cu^{II}]_2(O_2^{2-})^{2+}$  (**1b<sup>P</sup>**) similarly leads to the analogue tetramer cluster complex.<sup>55</sup>

## Summary and Conclusions

In this Article, we have described the copper(I), copper(II), and copper(I)–dioxygen chemistry with new tetradentate ligands possessing one imidazolyl donor ( $L^{MIm}$  and  $L^{EIm}$ ). The study is directed toward comparisons with our prior detailed investigations with TMPA–Cu chemistry.  $L^{MIm}$  containing Cu(I)–CO, mononuclear Cu(II), and the peroxo complex  $[(L^{MIm})Cu^{II}]_2(\mu-1,2-O_2^{2-})^{2+}$  (**1b<sup>P</sup>**) all show

structural and/or physical properties very similar to their TMPA–Cu analogues. However,  $L^{EIm}$  containing Cu(I)–CO, Cu(II) complexes (i.e., **2c**), and the peroxo complex  $[(L^{EIm})Cu^{II}]_2(\mu-1,2-O_2^{2-})^{2+}$  (**2b<sup>P</sup>**) are different; **2b<sup>P</sup>** possesses significantly weakened Cu–O and O–O bonds as compared to  $[(TMPA)Cu^{II}]_2(O_2^{2-})^{2+}$ . The relative decreases in bond strength are due to a square pyramidal distortion of **2b<sup>P</sup>**, which results in increased overlap (thus donation) of the ligand N's with the Cu(II)  $d_{x^2-y^2}$  orbital resulting in less donation from peroxo to Cu (decreased Cu–O bond strength) and increased electron density in the peroxo  $\pi^*_\sigma$  orbital (decreased O–O bond strength).

Future studies will address the electronic structures of copper complexes with these varied (in donor atom and tetradentate chelate architecture) tripodal tetradentate ligands, both from an experimental and theoretical perspec-

tive. Also, it will be of interest to compare complexes **1a** and **2a** in their kinetics and thermodynamics of copper(I)/O<sub>2</sub> reactivity giving superoxo–Cu(II) and peroxo–dicopper(II) complexes. Reactions of peroxo complexes employing tetradentate ligands with varied donor groups (i.e., S or O donors) will also be tested for their oxidative reactivity toward exogenous substrates.

**Acknowledgment.** K.D.K. and E.I.S. are grateful to the National Institutes of Health (Grants GM 28962 (K.D.K.) and DK 31450 (E.I.S.)) for support of this research.

**Supporting Information Available:** Crystallographic information files (CIF) for  $[(L^{MIm})Cu^{II}(CH_3CN)]^{2+}$  (**1c**),  $[(\mu_2-L^{EIm})_4-(Cu^{II})_4]^{4+}$  cluster, and  $[(L^{EIm})Cu^{II}(CH_3CN)(^-OCIO_3)]^+$  (**2c·OCIO<sub>3</sub>**). This material is available free of charge via the Internet at <http://pubs.acs.org>.